

Inorganic Ions in Glasses and Polycrystalline Pellets as Fluorescence Standard Reference Materials*

R. Reisfeld

Department of Inorganic and Analytic Chemistry, Hebrew University of Jerusalem, Jerusalem, Israel

(June 15, 1972)

The absorption and fluorescence of inorganic glasses and polycrystalline disks doped by heavy metal ions is discussed, and their use as fluorescence standards is evaluated. The advantages of the glass standards over other media is summarized.

The glass standards are divided into two groups (1) glasses doped by trivalent rare earths such as Gd^{3+} , Tb^{3+} , Eu^{3+} , Sm^{3+} , and Tm^{3+} which have narrow band optical spectra as a result of intraconfigurational transitions, and (2) glasses and polycrystalline disks doped by ions such as Tl^+ , Pb^{2+} , Ce^{3+} , and Cu^+ which have broad spectral bands since the optical spectra originate from interconfigurationally allowed transitions. Optical and physical parameters, including matrix effects, quantum efficiencies, decay characteristics, Stokes' shifts and spin-orbit versus orbit-lattice interactions due to the different transitions will be discussed.

Group (1) glasses are suitable for use as standards where a narrow well-defined fluorescence range is required, and group (2) glasses are suitable for use as standards whenever a substance with a wide range of fluorescence is measured. Special emphasis will be placed on energy transfer between donor and acceptor ions.

Key words: Fluorescence standards, inorganic ions; glass standards in fluorescence; rare-earth-doped glasses.

Introduction

The use of fluorescence and phosphorescence as experimental tools has increased immensely in the last decade. The fluorescence technique is used now as a common tool of research by physical chemists, physicists, analytical chemists, biochemists and biophysicists. The kinds of analyses which have been performed to date using fluorescence have varied, including such methods as trace metal determination, analysis for traces of organic materials and particularly for determination of trace constituents of biological systems. It provides some of the most sensitive and selective methods of qualitative and quantitative analysis. (Lower limits of detectability using fluorescence analysis lie often in subpart per million (ppm) and part per billion (ppb) range.) Fluorescence analysis especially, has many practical applications in the field of organic, inorganic, agricultural, biological and clinical chemistry.

The reader interested in the principles and applications of fluorescence in analysis is referred to two recently published books [1, 2]¹ on this subject and to a very comprehensive review on measurements of photoluminescence quantum yield in solutions written by Demas and Crosby. [3]

The following are a few examples in which fluorescence is used in health and environmental problems.

Organic Compounds

Many organic compounds fluoresce and/or phosphoresce and these properties have been widely used for analysis. An understanding of the basic aspects of the luminescence of organic compounds can greatly enhance its efficiency as an analytical tool.

The ability of proteins to luminesce has now been fairly thoroughly investigated and is mostly due to the presence of the fluorescent aromatic amino acids tryptophan and tyrosine, [4, 5]. Any biological process can be inhibited, stimulated or altered through photochemical methods by inducing electronic excited states in proteins and nucleic acids. In the investigation of these excited states by photoabsorption and luminescence techniques, a great deal of information can be obtained, not only about the number of biopolymeric molecules in the system, but also about their environment.

Significant qualitative and quantitative information concerning molecular structure can be obtained through fluorescence. When one considers that information of this kind can be obtained rapidly from the interior of the undamaged, usually functioning cell, one realizes the special importance of spectral lumi-

* This work was performed under NBS contract G-103.

¹ Figures in brackets indicate the literature references at the end of this paper.

nescence research techniques in biology. An example of fluorimetric methods in this area is: the fluorescent tags for labeling proteins [6] and amino acids [7-10] which have proven useful in immunochemistry, virology, bacteriology, parasitology, and mycology.

Agriculture

Determining factors in the degree of pest control by chemicals are (1) efficiency of application, (2) the loss by spray particle drift to immediate areas not intended to be treated, and (3) the effective life of the chemical on plants, animals and in soils after application. In this respect, fluorescence has made an outstanding contribution in pesticide analysis. The excitation and emission spectra, decay times, analytical curves, and limits of detection, have been obtained for many pesticides in media such as milk, animal feeds, fruits and vegetables, tissues, etc. [11]. Fluorescent tracer studies of spray and dust deposits on plants and soils have been reported [12, 13].

Biomedical Research

In this area, fluorescence spectroscopy has been used largely as an analytical tool for the assay of many materials of biological origin, [14] such as the examination of carcinogenic materials in the environment, [15] in metabolic studies of aromatic hydrocarbon carcinogens [16] and the determination of drugs, enzymes and proteins.

Of great interest are the experimental observations of the luminescence of cells and tissues in such pathological states as carcinogenesis, inflammation, psychic diseases and muscle atrophy due to denervation. Investigators have sought a correlation between luminescence intensity and the pathological process. However, more information about the structural chemical organization of the protoplasm during the development of the pathological process will be obtained if the comparison involves, not merely the intensity of the fluorescence of various cells, but the magnitude of the changes in fluorescence intensity due to several factors. The use of luminescence to a successfully selected set of experimental treatments will prove to be a useful technique in the field of molecular and cell biology and primarily in the field of practical medicine [17].

The mechanism of cancer induction by aromatic hydrocarbons is of particular interest and it is possible that the initial interaction is a complex formation between the hydrocarbon and a vital cell constituent, such as the nucleic acids which may be determined by changes in fluorescence spectra and parameters [18-20]. Various aromatic hydrocarbons may fluoresce at widely differing frequencies, a fact which is of considerable analytical importance. A history of fluorescence work with carcinogenic hydrocarbons was included in a lecture by Cook in 1950 [21]. Presently, fluorescence analysis is used in many studies to determine qualitatively and quantitatively the presence of

polynuclear hydrocarbons in the environment, usually after separation by thin-layer chromatography [22].

A method for binding dyes to nucleic acids is widely used in staining biological tissues for fluorescence microscopic examination and is used as a screening procedure for cancerous tissue [23].

Fluorometric techniques have made great inroads in the clinical laboratory as the basis of sensitive analytical methods [24, 25].

A. General

In all research and measurements in which fluorescence is involved, it is of utmost importance to measure the true wavelength (energy) of excitation and emission, and the fluorescence efficiency. To determine fluorescence efficiency directly, it is necessary to measure the rate of emission at all wavelengths and in all directions. In practice, this is a difficult measurement to perform with accuracy. In view of the difficulties associated with absolute methods, and the ease with which the fluorescence efficiency may be determined by reference to a standard, a search for a suitable standard is of great importance in spectrofluorimetry. The requirements for a good reference compound to be used as a standard are stringent. It should have a well-defined fluorescence and excitation spectrum, a relatively high quantum efficiency, it should be of the same geometry as the samples to be measured and should be stable. There should be little or no overlap between the absorption and the emission spectrum. The reference compound used in any instance should have its absorption and fluorescence in the same general region as the compound being studied. This last restriction is needed because most spectrofluorimeters record spectra which are not corrected for instrumental parameters.

Fluorescence measurements are mainly made on liquids in aqueous or organic solvents, using glass or quartz cuvettes, and in the solid phase with single crystals, in pellets [26] and in solvent glasses [27]. It would therefore be desirable that the standard reference material also be made of the same or similar material having a similar refractive index, thus avoiding the refractive index correction (discussed later). It is also essential that the standard have a small absorption, since a higher absorption introduces an error in the efficiency determination. This arises from the following consideration: The optically dilute measurement rests on Beer's Law $I_0B = I_0(1 - 10^{-AL})$ where B is the fraction of light absorbed by the sample, I_0 (quanta/sec · cm²) is the irradiance of incident light, A is the absorbance/cm, and L (cm) is the path length [3]. By expanding this expression in a power series we obtain $B = 1 - [1 - 2.303 AL] + [2.303 AL]^2/2 + \dots \approx 2.303 AL$. For solutions that are optically dilute, (absorbance less than 0.05) we can truncate the series and the following approximation is true: $B \approx 2.303 AL$. Thus at low solute concentrations, the fluorescence intensity is proportional to concentration.

With these criteria in mind we have attempted to prepare glass and pellet standards. The results of

our work are described in this paper. For the latest references to liquid standards the reader is referred to reference [3], for a sodium salicylate standard to reference [28], and for quantum yield determinations of powder phosphors to reference [29].

In this paper the physical parameters of doped glasses and alkali halides suggested as standards will be described. In order that such materials be used as standards, and the use be at optimal conditions for a fluorescence measurement, the following knowledge is needed:

1. Absorption and/or excitation spectrum.
2. Fluorescence spectrum.
3. Oscillator strength or molar absorptivity at the excitation wavelength.
4. Quantum efficiency for different excitation wavelengths.
5. Fluorescence output as a function of dopant concentration.
6. Lifetimes of fluorescence.
7. Quenching of fluorescence by additional processes such as energy transfer of radiation-induced color centers.
8. Stability.

The principles upon which the determination of quantum efficiencies is based will be discussed. Quantum yields of glasses and pellets prepared in this laboratory, for excitation to various electronic levels and the oscillator strengths of absorption to these levels will also be presented. The concentration dependence of quantum efficiency will be shown.

A short theory of the fluorescence of the material is also outlined for each group of proposed standards in order to simplify the choice of proper materials.

B. Determination of Quantum Yields

The luminescence quantum yield of a compound is defined as the fraction of excited molecules that luminesce after direct excitation by a light source.

The quantum yield, η , which is actually the ratio of probabilities of radiative transitions, $\sum A_i^r$ to the sum of the probabilities of radiative and nonradiative transitions, A_i^{nr} , is defined as:

$$\eta = \frac{\text{number of photons emitted}}{\text{number of photons absorbed}} = \frac{\sum A_i^r}{\sum A_i^r + \sum A_i^{nr}} \quad (1)$$

The quantum yield would equal unity if there were no nonradiative transitions.

The terms "quantum yield," "luminescence quantum efficiency," and "fluorescence yield" are used interchangeably.

Formula (1) serves as a basis of determination of quantum efficiency.

The determination of absolute quantum yields by this formula is difficult as mentioned in the introduction, hence a relative technique is often employed.

1. Comparative Method

Here, the fluorescence of an unknown is compared with the fluorescence of a compound whose fluorescence yield is well known. For dilute solutions, the following equation has been used [30]:

$$\eta_u = \eta_s \frac{n_u F_u A_s}{n_s F_s A_u} \quad (2)$$

where η_u and η_s are quantum yields of unknown and standard respectively, n the index of refraction, A the absorbance at the wavelength of absorption and F the integrated fluorescence output in quanta/unit wavelength. This equation is valid for equal numbers of photons incident on u and s . More often the following equation is used:

$$\eta_u = \eta_s \frac{F_u A_s I(\lambda_s) n_u^2}{F_s A_u I(\lambda_u) n_s^2} \quad (3)$$

In this equation, F is the integrated area under the corrected emission spectrum, and $I(\lambda)$ is the relative irradiance of the exciting light at wavelength λ . A is the absorbance.

Equations (2) and (3) differ in the ratio $\frac{n_u}{n_s}$ and $\frac{n_u^2}{n_s^2}$. As we see by comparison of the two formulae, refraction corrections can be substantial, modifying quantum yield results by factors of 2 or more. Therefore, one should be especially careful when applying the refractive index correction. A comprehensive discussion on this correction can be found in reference [3], p. 1018. As mentioned in the introduction, when the fluorescence of the unknown is compared with a standard of the same refractive index and geometry, the refractive index correction is avoided.

2. Determination of Quantum Yields from Lifetime Measurements

An alternative method is the determination of quantum yields by measurements of the lifetime of fluorescence and the natural lifetime of the state. Here we use the parameters appearing in eq (1)

$$\eta = \frac{\sum A_i^r}{\sum A_i^r + \sum A_i^{nr}} = \frac{\sum \frac{1}{\tau_{\text{nat}}}}{\frac{1}{\tau_{\text{exp}}}} = \sum \frac{\tau_{\text{exp}}}{\tau_{\text{nat}}} \quad (4)$$

where τ_{exp} is the experimentally determined lifetime from the level in question and $\sum \tau_{\text{nat}}^{-1}$ is the sum of natural lifetimes, corresponding to the sum of the inverse of the radiative transition rates from this level. One term, A_j^r , appearing in the sum $\sum A_i^r$ is equal to $\frac{1}{\tau_{\text{inat}}}$ and is obtained directly from the absorbance spectra as shown below. The other terms in the sum are then obtained from the relative areas

in the corrected emission spectra. A detailed example of these calculations is presented below for Eu(III) doped glasses.

The natural radiative lifetime is related to the Einstein coefficient of spontaneous emission. Using this relation, several authors developed expressions relating the natural lifetime of fluorescence to the absorption spectrum of the compound [31].

Here, a distinction can be made between two cases: 1. When the absorption and emission of a compound occur at close wavelengths, that is, zero or very small Stokes shifts are observed, and the spectrum is narrow as in the cases of rare earths in various media, one can use an approximation developed for atomic spectra. Using this approximation [32], one obtains for the natural lifetime the following expression, which is valid for a transition between two levels:

$$\tau_{\text{nat}}^{-1} = 2.880 \times 10^{-9} n^2 (g_1/g_u) \langle \nu^2 \rangle \int \epsilon(\nu) d\nu \quad (5)$$

where n is the index of refraction, $\langle \nu^2 \rangle$ the average squared wave number for the absorption maximum, g_u and g_1 the degeneracies in the upper and lower states, respectively, and $\epsilon(\nu)$ the molar absorptivity as a function of wave number.

In the case where there is a considerable Stokes shift between the absorption and emission as a result of strong vibronic coupling, for example in transition metal ions, mercury-like ions and organic compounds, a modified equation can be used for τ_{nat} [33], namely

$$\tau_{\text{nat}}^{-1} = 2.880 \times 10^{-9} n^2 \langle \nu_f^{-3} \rangle_{\text{av}}^{-1} \frac{g_1}{g_u} \int \frac{\epsilon(\nu) d\nu}{\nu} \quad (6)$$

The quantity $\langle \nu_f^{-3} \rangle_{\text{av}}^{-1}$ is given by

$$\langle \nu_f^{-3} \rangle_{\text{av}}^{-1} = \frac{\int F(\nu) \alpha \nu}{\int F(\nu) \nu^{-3} d\nu} \quad (7)$$

where $F(\nu)$ is the fluorescence output in photons as a function of wave number and ν is the wave number of $F(\nu)$.

3. Doped Glasses

The materials which we suggest as versatile standards for spectrofluorimetry and which were studied in this laboratory will be now described. They are divided in the text into four major groups: I. The rare-earth-doped glasses. II. Thallium-doped alkali halides. III. Glasses doped with thallium. IV. Glasses doped with Ce^{3+} , Pb^{2+} , and Cu^+ .

I. The Rare-Earth-Doped Glasses

The characteristic spectra of the trivalent rare earths are attributable to the presence of deep lying $4f$ shells in the ions. The electrons of these shells are screened by the outer shell electrons, and as a result

they give rise to a number of discrete energy levels. The presence of the surrounding lattice has little effect on the position of these levels; therefore, a close resemblance between the energy level diagram of the free ion and that of the incorporated ion exists (fig. 1).

Considerable attention has been paid in the past few years to the study of both the absorption and emission spectra of the rare earths [34, 35].

Trivalent rare-earth ions incorporated in inorganic solids exhibit luminescence owing to the intraconfigurational transitions of the $4f$ electron shell. The optical excitation of this luminescence can be governed by one of three possible mechanisms:

- excitation in the narrow $4f$ levels of the rare-earth ion;
- excitation in the broad levels due to $4f-5d^*$ transitions, or charge transfer processes;
- absorption of the host followed by energy transfer from the host to the rare earth activator.

While the first mechanism is operative in all the rare earths showing fluorescence, the second is well known mainly in europium and terbium. In the case of Eu^{3+} , this band is due to a charge transfer process between the Eu^{3+} ion and oxygen center. In the case of Tb^{3+} , however, the band is due to a $4f-5f$ transition in the Tb^{3+} ion. (Samarium also was found in some cases to exhibit a charge transfer type of excitation at wavelengths shorter than 220 nm.)

The narrow band emission of the trivalent rare earths in various media is always due to an inner f shell electronic transition. Intra- f -orbital transitions are parity forbidden in the free ion. In a solid, glass or liquid in the absence of a center of symmetry, the parity selection rule may be relaxed by the mixing of the $4f$ configuration with appropriate levels of configuration of opposite symmetry using odd terms in the static or dynamic crystal field expansion. There will also be an additional interaction owing to the influence of the crystal field of the host which produces broadening and splitting of the levels. As in the transition metal ions, which have been treated extensively by the ligand field theory, an increase in separation of a field-split degenerate level indicates an increase in the ligand field seen by the rare earth ion. The crystal field splittings in the rare earths are, however, much smaller than the transition ion splittings, and are not more than a few hundred wave numbers. For transitions between two nondegenerate levels, increasing the rare-earth-ligand interaction displaces both levels toward lower energies. The displacement of the upper, less shielded, level is usually greater, and thus the stronger perturbation causes shifts to longer wavelengths.

The electrostatic perturbation of a rare-earth ion should be directly related to its binding energy in the host medium. As a first approximation, this energy may be derived from a hard-sphere ionic model by the Born equation:

$$E = \sum \frac{Z_i Z_j}{r_{ij}} + \frac{b}{r^n} \quad (8)$$

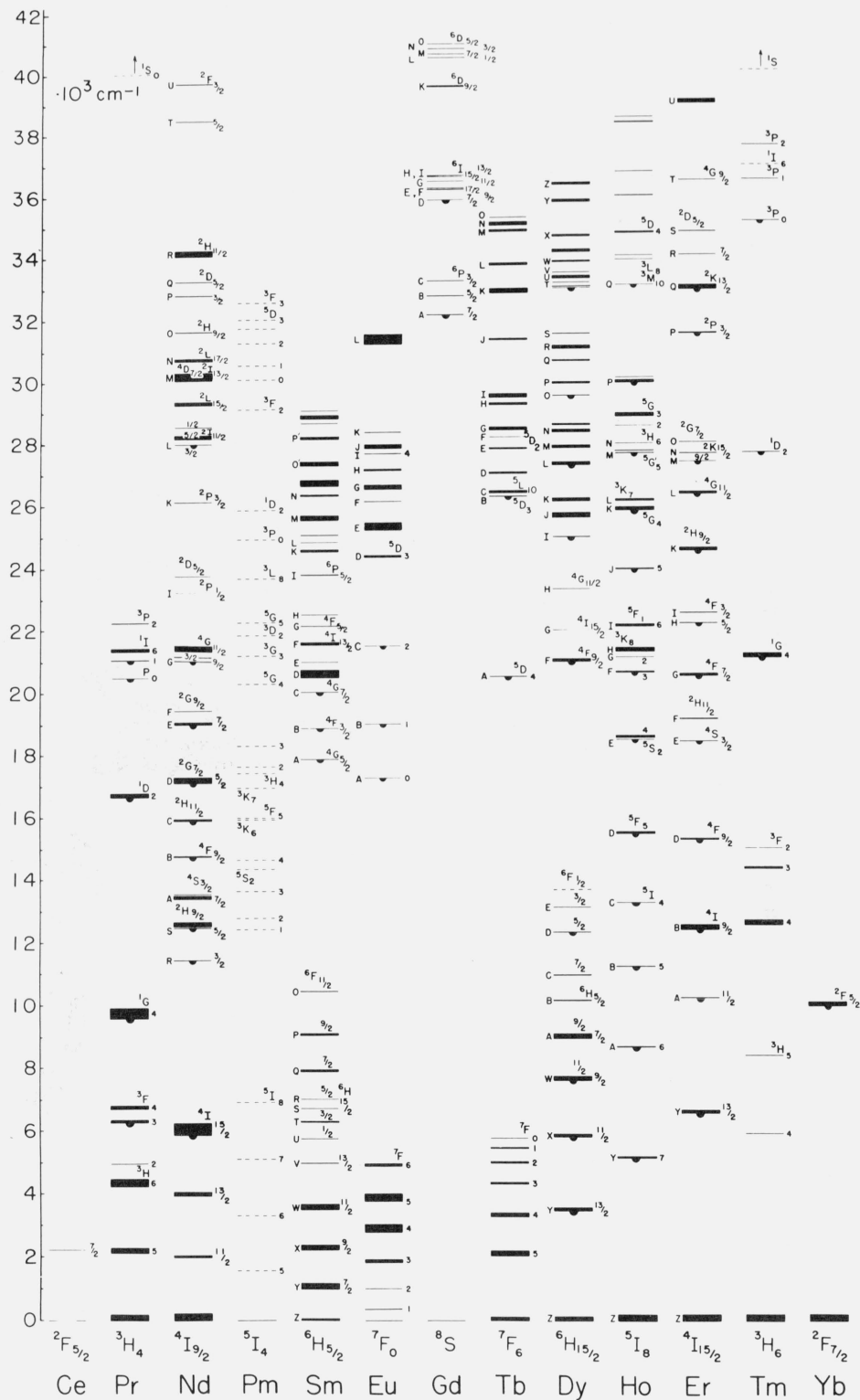


FIGURE 1. Energy level diagram of the rare-earth ions after G. H. Dieke, in Spectra and Energy Levels of Rare Earth Ions, H. M. Crosswhite and H. Crosswhite, Eds. (John Wiley & Sons, New York, N.Y., 1968), p. 142.

E = coulombic potential of the active ion; Z_i = charge on the active ion; Z_j = charge on the matrix ions; b = repulsion coefficient; r = distance between active ion and nearest anion; $n = 4$ to 10.

It was shown in a series of papers by Reisfeld et al. [36–40], that the behavior of rare earths in glasses is similar to that of rare earths in inorganic crystals of low symmetry except for inhomogeneous broadening of the spectra due to a multiplicity of rare-earth sites in glasses. According to our theory [39] a rare-earth ion occupies a center of a distorted cube comprised of four tetrahedra of borate, phosphate or silicate. Two oxygens belonging to such a tetrahedron produce an edge of the cube (fig. 2). The coordination

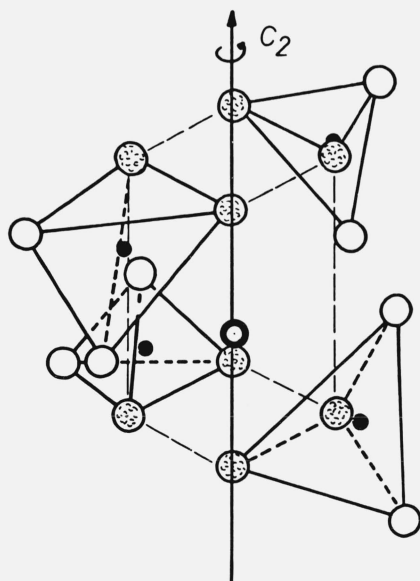
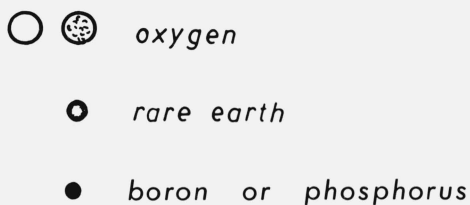


FIGURE 2. Proposed rare-earth site model.

of the rare earth in such an arrangement is with eight oxygens. The observed broadening in the spectrum can occur due to the existence of nonuniform, non-identical ligand fields caused by slightly different values of rare-earth oxygen distances. An average rare-earth oxygen distance was calculated by assuming a rare-earth sits in a center of a regular cube. In a cube made of borate tetrahedra, in which the boron-oxygen distance is 1.48 Å and the oxygen-oxygen distance 2.4 Å, the rare-earth oxygen distance is 2.1 Å. In a cube made of phosphate tetrahedra in which the phosphorus-oxygen distance is 1.57 Å and the oxygen-oxygen distance is 2.56 Å, the rare-earth oxygen distance is 2.22 Å. It should be realized that in

reality the symmetry is lower than cubic, and for the particular cases studied it was found to be of C_s symmetry Eu^{3+} in phosphate glass, [40] and C_2 for Tm^{3+} in phosphate and borate glasses [39]. As a result of this lower symmetry, forced electric dipole transitions become possible and absorption and fluorescence is observed.

The fluorescence can, in some cases, be quenched due to transfer of electronic excitation energy to the vibrations of the surrounding medium. Such interactions reduce the fluorescence quantum yield. In general the larger the energy difference between the two electronic states, the smaller the nonradiative transition probability between them [41]. For rare-earths, the energy difference between the electronic levels below which considerable quenching occurs is about four vibrational quanta (phonons). The non-radiative decay of the higher excited levels in the glasses is generally assisted by the phonons of the glass. The particular vibrational frequencies which are responsible for the quenching are the following:

bond	stretching frequency $\nu \text{ cm}^{-1}$	bond length Å
silicate, Si—O	1010–1115	1.62
metaphosphate, P—O	1140–1300	1.57
borate, B—O	1310–1380	1.39 (trigonal)
		1.48 (tetrahedral)

from which we conclude that in borate glasses, quenching will occur between levels that are separated by about 5000 cm^{-1} , while in silicate by about 4000 cm^{-1} .

We shall now show how this general theory works for specific cases.

A. Europium

The observed optical absorption and emission spectra of Eu^{3+} in glasses are characteristic of transitions between the lower energy levels of the $4f^6$ configuration of this ion. The oscillator strengths of the characteristic absorption bands in a phosphate glass together with the assignments of the transitions are given in table 1.

The oscillator strength was calculated from the well-known equation

$$f = 4.32 \times 10^{-9} \int \epsilon(\nu) d\nu \quad (9)$$

where ϵ is the molar absorptivity at the energy ν (cm^{-1}). The values of f presented in table 1 were corrected for population distribution of total concentration in \mathcal{F}_0 , \mathcal{F}_1 , and \mathcal{F}_2 . Using a Boltzmann distribution correction, the relative concentration for the three levels at room temperature were $C_0 = 0.792$, $C_1 = 0.200$ and $C_2 = 0.008$, respectively.

TABLE 1. Oscillator strengths and quantum yields of fluorescence of Eu^{3+} in phosphate glass

Transition assignment	Wave number cm^{-1}	Wavelength nm	Oscillator strength $\times 10^7$	Percent quantum yield of D_0 fluorescence
${}^7\text{F}_2 \rightarrow {}^5\text{D}_0$	16319	612.8	1.544	
${}^7\text{F}_1 \rightarrow {}^5\text{D}_0$	16771	592.2	0.351	
${}^7\text{F}_0 \rightarrow {}^5\text{D}_0$	17256	579.6	.006	0.95
${}^7\text{F}_1 \rightarrow {}^5\text{D}_1$	18700	534.7	.505	
${}^5\text{F}_0 \rightarrow {}^5\text{D}_1$	18993	526.4	.146	.91
${}^7\text{F}_0 \rightarrow {}^5\text{D}_2$	21493	465.3	1.248	.88
${}^7\text{F}_0 \rightarrow {}^5\text{D}_3$	24009	416.5	.547	.87
${}^7\text{F}_0 \rightarrow {}^5\text{L}_6$	25380	394.0	8.981	.87
${}^7\text{F}_1 \rightarrow {}^5\text{G}_5, {}^5\text{G}_6$	26041	384.0	6.019	
${}^7\text{F}_0 \rightarrow {}^5\text{G}_3$	26507	377.2	2.726	
${}^7\text{F}_1 \rightarrow {}^5\text{L}_8$	27285	366.5	.391	
${}^7\text{F}_0 \rightarrow {}^5\text{D}_4$	27567	362.7	1.926	
${}^7\text{F}_1 \rightarrow {}^5\text{H}_3$	30464	328.2	1.242	
${}^7\text{F}_1 \rightarrow {}^5\text{H}_5$	31152	321.0	3.001	
${}^7\text{F}_0 \rightarrow {}^5\text{H}_6$	31397	318.5	6.776	

Fluorescence was observed from the ${}^5\text{D}_0$ level and much weaker fluorescence (by a factor of three orders of magnitude) from the ${}^5\text{D}_1$ level. The corrected ${}^5\text{D}_0$ fluorescence to the ${}^7\text{F}$ ground state multiplet for Eu^{3+} in phosphate glass is given in figure 3. The corrected excitation spectrum of the fluorescence is also presented in this figure. The assignments, and relative intensities of the transitions are presented in table 2. (The transitions from the ${}^5\text{D}_0$ excited level to the ${}^7\text{F}_5$ and ${}^7\text{F}_6$ ground states are very weak, less than 1 percent of the total intensity, and are not included.) The ${}^5\text{D}_0 \rightarrow {}^7\text{F}_1$ emission band for Eu^{3+} are magnetic dipole-allowed transitions; the other

fluorescence bands arise from forced electric-dipole transitions. The large ratio of the fluorescence intensities for the ${}^5\text{D}_0 \rightarrow {}^7\text{F}_2$ and ${}^5\text{D}_0 \rightarrow {}^7\text{F}_1$ transitions implies a low symmetry field at the europium sites.

Quantum efficiencies of fluorescence from the ${}^5\text{D}_0$ level of Eu^{3+} in phosphate [41] and silicate glasses [42] were obtained by two independent methods, (a) lifetime measurements, and (b) comparison with a liquid standard.

a. Lifetime measurements. The quantum yield determination based on lifetime measurements is calculated from eq (4). The measured lifetime of the ${}^5\text{D}_0$ excited state in silicate glass was 2.69 ± 0.03 ms

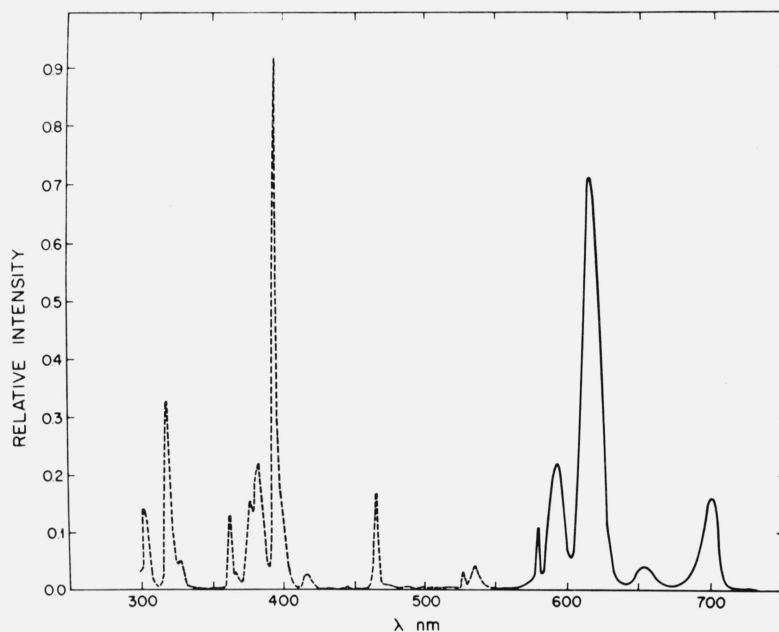


FIGURE 3. Corrected excitation (broken line) and emission (full line) spectrum of the ${}^5\text{D}_0$ fluorescence of Eu^{3+} in phosphate glass.

and in phosphate glass was 2.83 ± 0.03 ms.

The natural radiative lifetime was calculated using eq (5). In this equation, ϵ was corrected for the relative population of the 7F_0 level, which was taken as 0.771 in silicate and 0.792 in phosphate. Using the calculated value for $A({}^7F_0 \rightarrow {}^5D_0)$ the ratio of the intensities of fluorescence and the fact that $A({}^7F_0 \rightarrow {}^5D_0) = A({}^5D_0 \rightarrow {}^7F_0)$, the sum of radiative transition probabilities is expressed by:

$$\sum \frac{1}{\tau_{\text{nat}}} = \sum A_r = A({}^5D_0 \rightarrow {}^7F_0) \left[1 + \frac{S({}^5D_0 \rightarrow {}^7F_1)}{S({}^5D_0 \rightarrow {}^7F_0)} + \frac{S({}^5D_0 \rightarrow {}^7F_2)}{S({}^5D_0 \rightarrow {}^7F_0)} + \frac{S({}^5D_0 \rightarrow {}^7F_3)}{S({}^5D_0 \rightarrow {}^7F_0)} + \frac{S({}^5D_0 \rightarrow {}^7F_4)}{S({}^5D_0 \rightarrow {}^7F_0)} \right] \quad (10)$$

where S is the area of the relevant emission bands obtained from the corrected emission spectrum.

TABLE 2. Emission wavelength and relative areas of the ${}^5D_0 \rightarrow {}^7F_i$ transitions for Eu^{3+} in phosphate glass

Transition assignments	Wavelength	Relative fluorescence (areas)
${}^5D_0 \rightarrow {}^7F_0$	578.5	0.036
${}^5D_0 \rightarrow {}^7F_1$	591.9	1.000
${}^5D_0 \rightarrow {}^7F_2$	612.1	3.000
${}^5D_0 \rightarrow {}^7F_3$	654.7	0.219
${}^5D_0 \rightarrow {}^7F_4$	692.3	1.026

For Eu^{3+} in phosphate glass, the quantum yield obtained by this method was 0.95 [41] and for Eu^{3+} in silicate, 0.90 [42]. Europium-doped glasses do not show concentration quenching of the 5D_0 fluorescence [43].

b. Determination of Quantum Yield by Comparison Method. Here, the comparison was made with a solution of $\text{Eu}(\text{NO}_3)_3$ with a known quantum efficiency of 4 percent [41]. The fluorescence spectra were taken on a Turner Model 210 spectrofluorimeter² which gives corrected emission spectra in quanta/unit bandwidth, and excitation spectra corrected to constant energy [44]. The glasses were of the same geometry (standard cuvette form) as the cells in which the fluorescence of the solution of europium nitrate was measured.

Equation (11), which is a modification of eq (3) for use with a corrected spectrofluorimeter [45], was used:

$$\eta_u = \eta_s \left[\frac{(F_u A_s d_u \lambda_{\text{ex},s} n_s^2)}{(F_s A_u \lambda_{\text{ex},u} d_s \cdot n_s^2)} \right] \quad (11)$$

where all the symbols have the same meaning as in eq (3); subscripts u and s refer to the unknown and standard, respectively; d is the dilution factor denoting the ratio of the fluorescence species concentration in

the sample used for absorbance measurements to that used for fluorescence measurements; λ is the excitation wavelength.

The quantum efficiency determined by direct excitation to the 5D_0 level obtained by this method was 0.95 ± 0.03 for the phosphate glass, [41] and 0.93 ± 0.05 for the silicate glass [42].

The very similar values for the quantum yield obtained by the two independent methods suggests use of the phosphate glass as a reliable fluorescence standard at wavelengths similar to those for the fluorescence of europium, as summarized in table 2. To obtain this quantum efficiency, it is necessary to excite the 5D_0 level of europium from the 7F_0 level at 580 nm, or from the 7F_1 level at 591 nm. Excitation to higher levels results in a decrease of fluorescence yield from the 5D_0 level, as additional paths for radiative and nonradiative transitions become possible.

The quantum yields of fluorescence upon excitation to selected levels in phosphate glass are presented in table 1 [41]. The values of quantum efficiencies for fluorescence monitored by 5D_0 emissions when excited to higher levels, as listed in the table, were obtained from the ratio of the area under the excitation spectrum to the ratio of the area under the absorption band for a given level using eq (12). No corrections were made for the change of refractive index with wavelength.

$$Q.Y.^b = \frac{F_b/A_b \lambda_{\text{ex},a}}{F_a/A_a \lambda_{\text{ex},b}} Q.Y.^a \quad (12)$$

- $Q.Y.^b$ Quantum efficiency of 5D_0 fluorescence by excitation to a given level
 $Q.Y.^a$ Quantum efficiency of 5D_0 fluorescence by excitation to the 5D_0 level
 F_b peak area of a given level in excitation spectrum
 A_b peak area of a given level in the absorption spectrum
 F_a peak area of 5D_0 in excitation spectrum
 A_a peak area of 5D_0 is absorption spectrum
 $\lambda_{\text{ex},a}$ wavelength of 5D_0 absorption (581 nm)
 $\lambda_{\text{ex},b}$ wavelength of absorption for given transition.

Therefore, europium glass is proposed as a standard where the emission of the unknown is close to the emission of Eu^{3+} (table 2) and the excitation wavelength is also near one of the excitation wavelengths of europium (table 1).

The fluorescence of europium shows a linear dependence on concentration up to 7 weight percent and no quenching is observed. Therefore, the concentration of the standard used will be governed by the desired wavelength of excitation because of different oscillator strengths. For excitation at 580 or 591 nm, 1–2 weight percent of Eu^{3+} in glass is suggested. The europium glass standard is suitable for compounds having narrow fluorescence in the wavelength range of 600–700 nm.

² In order to adequately describe materials and experimental procedures, it was occasionally necessary to identify commercial products by manufacturer's name or label. In no instances does such identification imply endorsement by the National Bureau of Standards, nor does it imply that the particular product or equipment is necessarily the best available for that purpose.

B. Gadolinium

Gadolinium has a comparatively simple optical absorption and emission spectrum because the trivalent gadolinium has a half-filled configuration corresponding to $7-4f$ electrons. The ground state is $^8S_{7/2}$, which is not split in a crystal field. Its first excited state lies around 3200 cm^{-1} , which corresponds to the 312 nm band. Gadolinium is the only rare-earth ion whose spectrum consists only of bands lying in the UV region. The emission spectrum of gadolinium in borate glass [46] has a major band with maximum at 312 nm due to the $^3P_{7/2}-^8S_{7/2}$ transition (fig 4), which is essentially unchanged in other

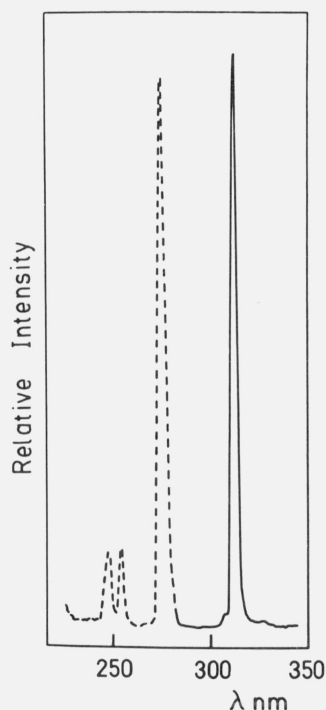


FIGURE 4. Corrected excitation (broken line) and emission (full line) spectrum of the $^6P_{7/2}$ fluorescence of Gd^{3+} in borate glass.

matrices [47]. The oscillator strength of this transition and of transitions to higher levels from $^6P_{7/2}$ are tabulated in table 3. The quantum yield of the 312 nm fluorescence was computed by taking a ratio of the measured lifetime of $^6P_{7/2}$ fluorescence, which is 4.10 ± 0.01 ms, to the natural lifetime of this transition obtained by use of formula (5). The calculated lifetime was found to be 4.10 ms. The quantum yield thus obtained equals 1 with an estimated error of ± 1 percent. The quantum yield of $^6P_{7/2}$ fluorescence at excitation to higher levels was obtained relative to the quantum yield of excitation at $^6P_{7/2}$ using eq (12).

The quantum efficiencies of the 312 nm fluorescence of gadolinium in borate glass are tabulated in table 3.

Borate glass containing gadolinium can be used as a standard for fluorescent materials having emissions around 312 nm and excitation peaks around 250 and 273 nm. Because of the narrowness of the band, it is suitable for materials with narrow fluorescence. Gadolinium in borate glass shows a linear fluorescence output as a function of concentration from the ppm range [48] to 7 weight percent (the highest concentration introduced).

C. Terbium

The electronic configuration of Tb^{3+} is $4f^8$. The absorption spectrum of Tb^{3+} arises from the transitions from the ground 7F_6 state to higher levels of the f orbital giving rise to sharp bands of absorption due to $f-f^*$ transitions. In glasses, an additional broad band occurs in the UV due to the $4f^8 \rightarrow 4f^7 5d$ transition. The oscillator strengths of Tb^{3+} together with the quantum efficiencies of the 5D_4 level are presented in table 4.

Terbium fluorescence is observed in the glass from the 5D_4 and 5D_3 excited states. The 5D_3 fluorescence, around 378–369 nm, is quenched at higher concentrations of Tb^{3+} due to $Tb^{3+} - Tb^{3+}$ interactions. The 5D_4 fluorescence consists of seven bands due to the transitions: $^5D_4 \rightarrow ^7F_{6,5,4,3,2,1,0}$. The wavelengths for maxima of these bands together with their relative peak areas are presented in table 5. The corrected emission

TABLE 3. Oscillator strengths and quantum yields of fluorescence of Gd^{3+} in borate glass

Transition assignment	Wavelength nm	Wave number cm^{-1}	Oscillator strength $\times 10^6$	Quantum yield of $^6P_{7/2}$ fluorescence					
$^8S_{7/2} \rightarrow ^6P_{7/2}$	313.0	31949	0.176	1					
$^6P_{5/2}$	307.0	32573	.074						
$^6I_{7/2}$	280.25	35682	.117						
$\left\{ \begin{array}{l} ^6I_{9/2} \\ ^6I_{7/2} \\ ^6I_{11/2} \end{array} \right.$	277.0	36101	.781						
					$^6I_{13/2}$	274.3	36456	1.679	0.870
					$^6I_{15/2}$				
$^6D_{9/2}$	253.6	39432	0.406	.735					
$^6D_{7/2}$	247.6	40388	.385	.735					
$^6D_{3/2}$									
$^6D_{5/2}$	245.5	40733	.099	.590					

TABLE 4. Oscillator strengths and quantum yields of 5D_4 fluorescence of Tb^{3+} in borate glass

Transition assignment	Wavelength nm	Wavenumber cm^{-1}	Oscillator strength $\times 10^7$	Quantum yield
$^7F_6 \rightarrow ^5D_4$	485.5	20597	0.633	1
5D_3	378.9	26392	3.812	0.60
5G_6				
$^5L_{10}$				
5G_5	352.5	28369	7.622	.62
5G_2				
5G_4				
5L_9				
5G_3				
5L_8	340.6	29360	5.764	.256
5L_7				
5L_6				
5G_2				
5D_1				
5D_0	318.5	31397	4.405	.197
5H_7				
5H_6				
5H_4	303.4	32960	5.249	.06
5H_5				
5H_3				
5I_8				
5F_4				
$4f^8 \rightarrow 4f^2 5d$	220.5	45351	385×10^4	

TABLE 5. Emission wavelength and relative areas of the 5D_4 level of Tb^{3+} in borate glass

Transition assignments	Wavelength nm	Relative fluorescence (areas)
$^5D_4 \rightarrow ^7F_6$	486	0.040
$^5D_4 \rightarrow ^7F_5$	541	.150
$^5D_4 \rightarrow ^7F_4$	585	.033
$^5D_4 \rightarrow ^7F_3$	624	.019

spectrum from the 5D_4 level and the corrected excitation spectrum are presented in figure 5.

No quenching of the 5D_4 terbium fluorescence was observed in our work with borate glasses from the ppm range to 6 weight percent [49].

The lifetime of the 5D_4 fluorescence of terbium follows a simple exponential with an e^{-1} decay time of 2.80 ± 0.05 ms.

The quantum yields of 5D_4 fluorescence on excitation to this level were obtained using the measured

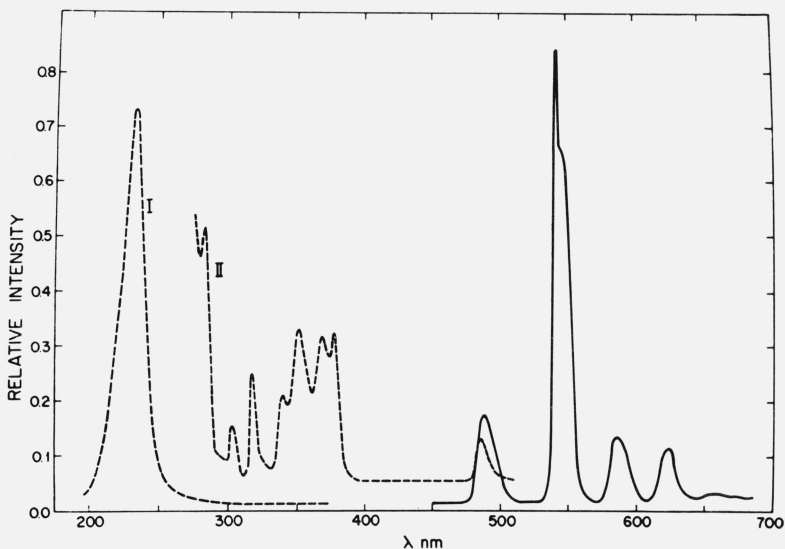


FIGURE 5. Corrected excitation (broken line) and emission (full line) spectrum of the 5D_4 fluorescence of Tb^{3+} in borate glass. I = the intensity decreased by a factor of 30.

lifetime and absorption and emission spectra in a similar way as the quantum yields for europium, using eqs (4), (5), and (10).

The radiative probability for the ${}^7F_6 \rightarrow {}^5D_4$ transition was calculated using eq (5) and equals 57.6 s^{-1} .

The total radiative transition probability, from the 5D_4 level, $\sum A_i^r [{}^5D_4]$ is given by:

$$\sum A_i^r [{}^5D_4] = \sum_{i=0}^6 A [{}^5D_4 \rightarrow {}^7F_i].$$

From the emission spectrum we found that

$$\sum A_i^r [{}^5D_4] = 6A [{}^5D_4 \rightarrow {}^7F_6];$$

thus, the total radiative transition rate from the 5D_4 level is 345 s^{-1} , which is equivalent to

$$\left[\sum \frac{1}{\tau_{nat}} \right]^{-1}$$

2.9 ms. Hence the quantum yield

$$\text{Q.Y.} = \frac{2.8}{2.9} = 0.97$$

with an estimated error of about 3 percent.

The quantum yields of the 5D_4 level on excitation to higher levels were obtained as they were for Eu^{3+} and Gd^{3+} ; i.e., by taking ratios of the areas under the excitation spectrum to the areas in the absorption spectra, and multiplying by the ratio of excitation wavelength at 480 to the wavelength for the given excitation. Equation (12) was used for this calculation.

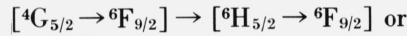
Terbium can be used as a standard for compounds

which fluoresce at approximately 480, 543, 587, and 624 nm.

D. Samarium

The electronic configuration of Sm^{3+} is $4f^5$. Its absorption spectrum arises from transitions from the ground ${}^6H_{5/2}$ level to higher levels of the $4f^5$ configurations. The oscillator strengths of Sm^{3+} in phosphate glass are presented in table 6.

The excitation and emission spectra of Sm^{3+} in phosphate glass are presented in figure 6. The visible fluorescence of Sm^{3+} arises from the transitions from the ${}^4G_{5/2}$ level to the ground 6H multiplet. The relative fluorescence intensities to each level in the multiplet are presented in table 7. The fluorescence arising from these transitions is linear with concentration up to about 0.6 weight percent. At higher concentrations an ion-ion energy transfer occurs. This multipolar interaction can be represented systematically (see ref. [35], p. 97):



Therefore, if samarium glass is to be used as a fluorescence standard for the wavelength range presented in table 7, a glass containing less than 0.6 weight percent of this element should be used.

The quantum yield of the ${}^4G_{5/2}$ fluorescence of samarium in phosphate and borate glasses was calculated by use of eqs (4), (5), and (10). The radiative transition probability from ${}^6H_{5/2}$ to ${}^4G_{5/2}$ in phosphate glass as obtained from the absorption spectrum, using eq (5), is 41.3 s^{-1} . The total radiative transition probability from the ${}^4G_{5/2}$ level, $\sum A_i^r [{}^4G_{5/2}]$, is given by

TABLE 6. Oscillator strengths and quantum yields of ${}^4G_{5/2}$ fluorescence of Sm^{3+} in phosphate glass

Energy level	Wave number cm^{-1}	Wavelength nm	Oscillator strength $\times 10^6$	Quantum yields
${}^4G_{5/2}$	17467-18348	545.0-572.5	0.0476	0.950
${}^6F_{3/2}$	18779-19047	525.0-532.5	.0115	
${}^4G_{7/2}$	19800-20100	497.5-505.0	.0183	
${}^4I_{9/2}$, ${}^4M_{15/2}$, ${}^4I_{11/2}$	20181-21621	462.5-496.0	1.5370	.653
${}^4I_{13/2}$	21267-21978	455.0-470.0	0.1388	
${}^4F_{5/2}$	21978-22346	447.5-455.0	.0273	.491
${}^4M_{17/2}$, ${}^4G_{9/2}$, ${}^4I_{15/2}$	22321-23255	430.0-448.0	.2169	
(6P , 4P) $_{5/2}$	23255-24630	406.0-430.0	1.0039	.213
${}^4L_{17/2}$, ${}^6F_{7/2}$, ${}^6P_{3/2}$	24242-25316	395.0-412.5	4.0749	.264
${}^4K_{11/2}$, ${}^4M_{21/2}$, ${}^4L_{15/2}$				
${}^4G_{11/2}$, ${}^4D_{1/2}$, ${}^6P_{7/2}$	25252-26109	383.0-396.0	0.2298	.249
${}^4L_{17/2}$, ${}^4K_{13/2}$, ${}^6F_{9/2}$	26109-27173	368.0-383.0	1.2246	.224
${}^4D_{3/2}$, (4D , 6P) $_{3/2}$	27173-28089	356.0-368.0	1.2230	.226
${}^4H_{7/2}$	27972-28368	352.5-357.0	0.0264	
${}^4K_{15/2}$, ${}^4H_{9/2}$, ${}^4D_{7/2}$				
(4K , 4L) $_{17/2}$, ${}^4L_{19/2}$	28490-29450	340.0-351.0	.7457	.155
${}^4H_{11/2}$				

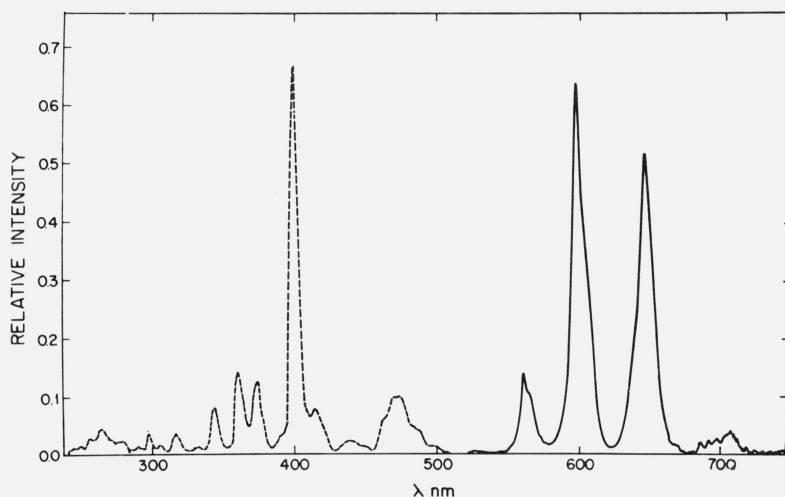


FIGURE 6. Corrected excitation (broken line) and emission (full line) of the ${}^4G_{5/2}$ fluorescence of Sm^{3+} in phosphate glass.

TABLE 7. Emission wavelength and relative areas of fluorescence from the ${}^4G_{5/2}$ level of Sm^{3+} in phosphate glass

Transition assignments	Wavelength nm	Relative areas
${}^4G_{5/2} \rightarrow {}^6H_{5/2}$	562	1.000
${}^4G_{5/2} \rightarrow {}^6H_{7/2}$	597	5.128
${}^4G_{5/2} \rightarrow {}^6H_{9/2}$	645	4.856
${}^4G_{5/2} \rightarrow {}^6H_{11/2}$	707	0.574
${}^4G_{5/2} \rightarrow {}^6H_{13/2}^*$	830	0.487
${}^4G_{5/2} \rightarrow {}^6H_{15/2}^*$	900	

* These two transitions were obtained by calculation assuming quantum yield of level ${}^4G_{5/2}$ to be 0.95.

$$\sum A_i I_i [{}^4G_{5/2}] = \sum_{i=5/2}^{15/2} {}^4G_{5/2} \rightarrow \sum {}^6H_i.$$

The measured lifetime of the fluorescence from the ${}^4G_{5/2}$ level is 1.91 ms. By assuming the quantum efficiency of fluorescence from this level to be 0.95, we can calculate the transition rate ${}^4G_{5/2} \rightarrow {}^6H_{13/2}$, ${}^6H_{15/2}$, which is out of the range of measurements, by use of the formula³

$$Q.Y. = \tau_{\text{exp}} \left[A({}^6H_{5/2} \rightarrow {}^4G_{5/2}) \times (1 + \frac{A({}^4G_{5/2} \rightarrow {}^6H_{7/2})}{A({}^6H_{5/2} \rightarrow {}^4G_{5/2})} + \frac{A({}^4G_{5/2} \rightarrow {}^6H_{9/2})}{A({}^6H_{5/2} \rightarrow {}^4G_{5/2})} + \frac{A({}^4G_{5/2} \rightarrow {}^6H_{11/2})}{A({}^6H_{5/2} \rightarrow {}^4G_{5/2})} + x) \right]$$

$$0.95 = 0.00191[41.3(1.000 + 5.128 + 4.856 + 0.5744 + x)].$$

$$x = \frac{A({}^4G_{5/2} \rightarrow {}^6H_{13/2})}{A({}^6H_{5/2} \rightarrow {}^4G_{5/2})} + \frac{A({}^4G_{5/2} \rightarrow {}^6H_{15/2})}{A({}^6H_{5/2} \rightarrow {}^4G_{5/2})}$$

The numbers in parenthesis are the relative fluorescence intensities of the transitions ${}^4G_{5/2} \rightarrow {}^6H_i$ as given in table 7. The relative areas of ${}^4G_{5/2} \rightarrow {}^6H_{13/2}$, ${}^6H_{15/2}$ thus calculated amount to about 4 percent of the total emission of the ${}^4G_{5/2}$, hence the assumption that the quantum yield equal 0.95 is justified. The estimated error in Q.Y. here is about 3 percent.

The quantum yields of the ${}^4G_{5/2}$ fluorescence on excitation to higher levels were calculated by eq (12) using as an internal standard the fluorescence yield on direct excitation to the ${}^4G_{5/2}$ level. They were independently calculated by use of Eu^{3+} glass as standard. The values of quantum yield are presented in table 6.

Glasses containing small concentrations of Sm^{3+} can be used as fluorescence standards for compounds which fluoresce at around 560, 602, and 640 nm.

By examining the quantum efficiencies of Eu^{3+} , Gd^{3+} , Tb^{3+} , and Sm^{3+} in glasses, we see that the fluorescence quantum yields from the lowest excited fluorescing levels approach unity. This is because the differences between these levels and the ground levels (or multiplets) are more than five phonons. In such cases, the electronic transitions are almost totally radiative.

E. Thulium

The electronic configuration of trivalent thulium is $4f^{12}$. It possesses more than one strongly emitting level and selective excitation of the various fluorescent levels have been achieved in both phosphate and borate glasses [50]. Because part of the fluorescence occurs in the infrared, we were unable to obtain the relative quantum efficiency of fluorescence of thulium for various levels. It was found, however, that an estimation of an "apparent quantum efficiency" of these glasses could be of practical use if the materials are used as fluorescence standards. Therefore, these parameters will be presented here.

Oscillator strengths of Tm^{3+} in phosphate and borate glasses are presented in table 8. They were obtained by gaussian analysis of the absorption spectrum.

TABLE 8. Oscillator strengths, f , of Tm^{3+} in borate and phosphate glasses

Transition assignments	Borate			Phosphate		
	Wave number cm^{-1}	Wavelength nm	$f \times 10^6$	Wave number cm^{-1}	Wavelength nm	$f \times 10^6$
$^3H_6 \rightarrow ^3H_4$	5847 to 6134	1630.0 to 1710.0	3.94	5714	1750.0
$^3H_6 \rightarrow ^3H_5$	8257	1211.0	2.09	8250	1212.0	1.82
$^3H_6 \rightarrow ^3F_4$	12626 to 12903	792.0 to 775.0	4.39	12626	792.0	3.00
$^3H_6 \rightarrow ^3F_3$	14619	684.0	4.02	14550	687.2	2.53
$^3H_6 \rightarrow ^3F_2$	15100	662.0	0.70	15060	664.0	0.22
$^3H_6 \rightarrow ^1G_4$	21231 to 21505	471.0 to 465.0	2.19	21052	475.0	1.58
				21505	465.0	
$^3H_6 \rightarrow ^1D_2$	27855 to 28050	356.5 to 355.0	3.75	27855	359.0	3.06
$^3H_6 \rightarrow ^1I_6$	34246 to 34662	292.0 to 288.5	4.14	33057	302.5	31.87
				34364	291.0	
$^3H_6 \rightarrow ^3P_0$	35082	285.0		35057	286.0	
$^3H_6 \rightarrow ^3P_1$	36363	275.0		36166	276.5	
$^3H_6 \rightarrow ^3P_2$	37950 to 38387	262.5 to 260.5	6.13	38095	262.5	14.46

The absorption occurs from the ground 3H_6 state. The excitation spectrum of the 453 nm fluorescence The emission spectra of Tm^{3+} at various excitation wavelengths are presented in table 9.

TABLE 9. Emission spectrum of Tm^{3+} at various excitation wavelengths

Excitation (nm)	Assigned transition	Emission			
		borate		phosphate	
		λ (nm)	R.A.*	λ (nm)	R.A.*
468.0(1G_4)	$^1G_4 \rightarrow ^3H_4$			651.50	1.000
	$^1G_4 \rightarrow ^3H_5$			752.75	0.114
	$^3F_2 \rightarrow ^3H_6$			665.50	.083
	$^3F_3 \rightarrow ^3H_6$			690.00	.708
358.0(1D_2)	$^1D_2 \rightarrow ^3H_4$	456.00	1.000	453.00	1.000
	$^1D_2 \rightarrow ^3H_5$	517.00	0.008	513.00	0.011
	$^1D_2 \rightarrow ^3F_4$	665.00	.127	663.50	.034
	$^1G_4 \rightarrow ^3H_6$	478.00	.118	478.00	.063
	$^1G_4 \rightarrow ^3H_4$	652.50	.180	651.50	.074
	$^3F_2 \rightarrow ^3H_6$	665.50	.014	665.50	.009
288.0(3P_0)	$^1I_6 \rightarrow ^3H_4$	355.00	.446	350.00	1.000
	$^1I_6 \rightarrow ^3H_5$	385.00	.125	383.00	0.094
	$^3P_0 \rightarrow ^3F_4$	465.00	.155	463.00	.200
	$^1I_6 \rightarrow ^3F_4$				
	$^1I_6 \rightarrow ^3F_3$	500.00	.110	498.00	.060
	$^3P_0 \rightarrow ^3F_3$	530.00	.061	521.50	.094
	$^1I_6 \rightarrow ^3F_2$				
	$^3P_0 \rightarrow ^1G_4$	705.00	.754	701.00	1.000
	$^1I_6 \rightarrow ^1G_4$				
	$^1D_2 \rightarrow ^3H_5$	367.50	.275	365.00	0.133
	$^1D_2 \rightarrow ^3H_4$	456.00	1.000	453.00	.455
	$^1D_2 \rightarrow ^3H_5$	517.00	0.067	513.00	.044
$^1D_2 \rightarrow ^3F_4$	
$^1G_4 \rightarrow ^3H_6$	480.00	.190	478.00	.105	
$^1G_4 \rightarrow ^3H_4$	
$^3F_2 \rightarrow ^3H_6$	
$^3F_3 \rightarrow ^3H_6$	

*Relative areas; for each excitation the areas are given relatively to the strongest emission band which is taken as unity.

($^1D_2 \rightarrow ^3H_4$) and the emission spectrum with excitation at 262 nm ($^3H_6 \rightarrow ^3P_0$) are presented in figure 7.

The "apparent quantum yield," (A.Q.Y.), of 450–478 nm fluorescence of Tm^{3+} was calculated by the comparative method, using Tb^{3+} as a standard. The A.Q.Y. of Tm^{3+} is defined by eq [12a]:

A.Q.Y. Tm^{3+}

$$= \left\{ \frac{F [(^1G_4 \rightarrow ^3H_6) + (^1D_2 \rightarrow ^3H_4)] [A(^7F_6 \rightarrow ^5D_4)]}{\left[F \left(^5D_4 \rightarrow \sum_{i=6}^{i=0} ^7F_i \right) A(^3H_6 \rightarrow ^1D_2) \right]} \right\} \text{ (Q.Y. } Tb^{3+}) \quad [12a]$$

in which $F[(^1G_4 \rightarrow ^3H_6) + (^1D_2 \rightarrow ^3H_4)]$ is the sum of the corresponding fluorescence intensities (expressed as areas under the emission spectrum) of Tm^{3+} ; $A(^3H_6 \rightarrow ^1D_2)$ is the absorbance for the 358 nm band of Tm^{3+} ; $F(^5D_4 \rightarrow \sum ^7F_i)$ is the sum of fluorescence intensities of the 5D_4 fluorescence of Tb ; $A(^7F_6 \rightarrow ^5D_4)$ is the absorbance for the Tb^{3+} band at 358 nm; and Q.Y. Tb^{3+} is the quantum efficiency of Tb^{3+} taken as 0.63. The apparent quantum efficiency for 10 weight percent of Tm^{3+} , calculated in this way, is 0.037 in borate and 0.043 in phosphate glasses.

Here, not all the transitions of Tm^{3+} were taken into account, but since the relative transitions to each level are constant for a given host, Tm^{3+} doped glasses can be used as standards for fluorescence around 450–480 nm and excitation around 358 nm. This small value of A.Q.Y. is not surprising since it is known [50] that at one weight percent of Tm^{3+} the concentration quenching of fluorescence is about 50 percent due to multipolar transitions between neighboring thulium ions. It should also be remembered that the fluorescence around 455–475 nm is one of seven transitions from

1D_2 and one of the six 1G_4 transitions.

Because of its low A.Q.Y. value, use of Tm^{3+} in the region of 450–480 nm fluorescence has no obvious advantage over Tb^{3+} as a standard. However, it can be used as an internal standard for Tm^{3+} . This fluorescence can be used to determine the apparent yield at 355 nm ($^1I_6 \rightarrow ^3H_4$), 385 nm ($^1I_6 \rightarrow ^3H_5$) and 367 nm ($^1D_2 \rightarrow ^3H_6$), upon excitation to 288 nm (3P_0) or 265 nm (3P_2), which is of practical value as a standard in the UV region.

II. Thallium-Doped Alkali Halides and Glasses

While the rare-earth ions have characteristic sharp fluorescence bands largely independent of the host, due to $f-f^*$ transitions, mercury-like ions in general and thallium in particular have much broader fluorescence, with the fluorescence maxima strongly dependent on the composition of the host matrix. The quantum efficiency also is dependent on the host as described below. Monovalent thallium is a well-known fluorescence emitter in the UV region and was used in our studies in various matrices as a possible standard for UV fluorescence.

The absorption spectrum of thallium consists of three main bands: A, B, and C. A review of the absorption and luminescence of this element can be found in references [51] and [52]. The absorption band A, which is discussed here, is assigned to the spin-forbidden transition $^1A_{1g} \rightarrow ^3T_{1u}$ ($^1\Gamma_1 - ^3\Gamma_4^o$), equivalent to $^1S_0 \rightarrow ^3P_1$ in the free thallos ion (see fig. 8), which is triply degenerate. It can be split in a cubic field by a dynamic Jahn-Teller effect [54], or the degeneracy can be lifted when the symmetry is decreased in glasses [55] from cubic to tetragonal or lower. The oscillator strengths, f , for the maxima of the A bands are presented in table 10. It was shown by Scott and Hu [53] that when the chloride ligand is replaced by an oxygen ligand in aqueous solution, the maxima of the band is shifted towards a shorter wave-

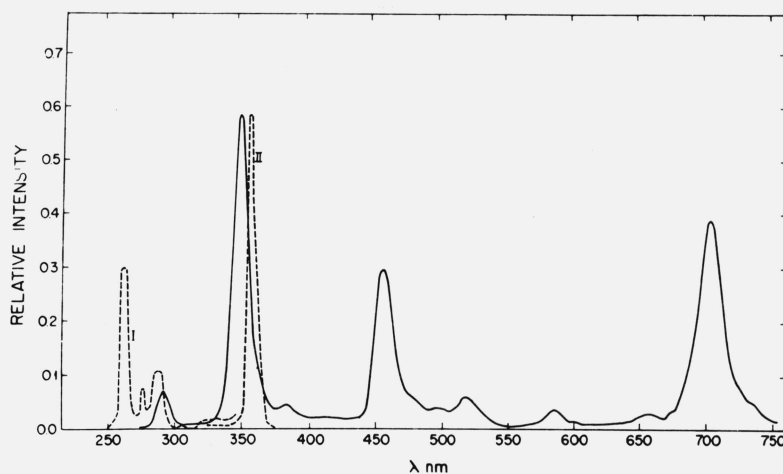


FIGURE 7. Corrected excitation spectrum of the 1D_2 fluorescence (broken line—II decreased by a factor of 2) and emission spectrum (full line) excited at 3P_2 band of thulium in phosphate glass.

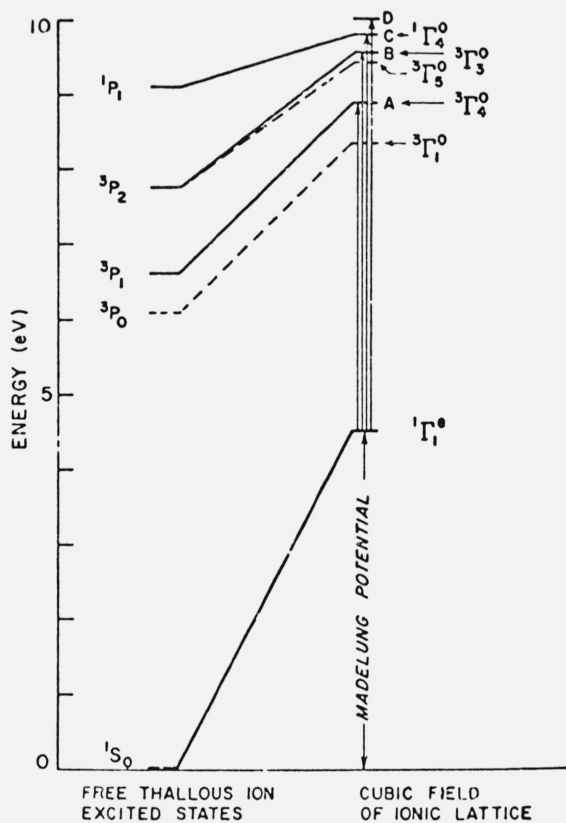


FIGURE 8. The energy of thallous ion in a cubic field.

length. The fluorescence occurs at a somewhat longer wavelength due to the Stokes' shift.

The relation between absorption and fluorescence can be most easily explained by the use of the configurational coordinate diagram, given in figure 9 [56]. The potential energy of the luminescent center in a crystal lattice is plotted here as a function of the configurational coordinate r . The quantity r represents a mean distance between the luminescence center and the surrounding ligands. The horizontal lines represent the vibrational states of the metal-oxygen bond vibrations.

At a temperature of absolute zero the luminescent center will occupy the lowest vibrational level of the ground state. The ions surrounding the central ion vibrate about their equilibrium positions situated at a distance r_0 from the central ion. At higher tempera-

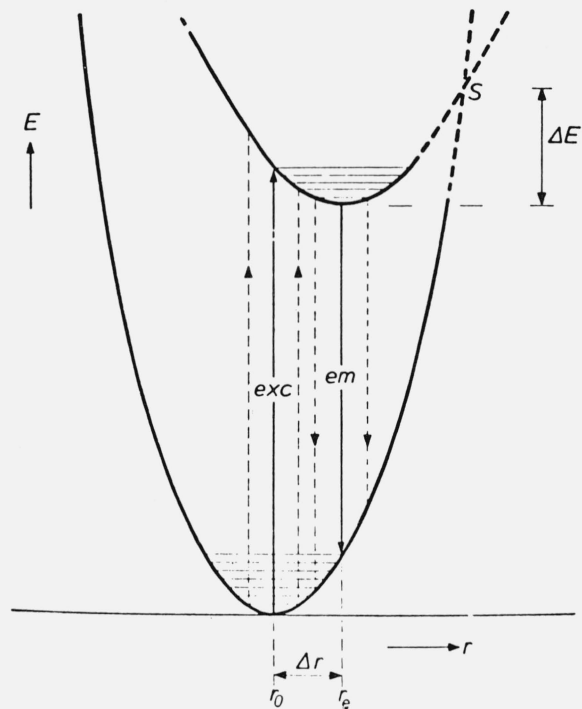


FIGURE 9. Configurational coordinate diagram of a luminescent center. The potential energy E of the center in the lattice is plotted as a function of the configurational coordinate r for the ground state and the first excited state. In practice, r is identified with the distance between the central cation and the surrounding anions. Vibrational states are represented schematically by horizontal lines in the parabolae. The excitation and emission transitions correspond to vertical transitions between the two curves. Since $\Delta r \neq 0$, the emission shows a Stokes' Shift (wavelength of the emission is longer than that of the excitation). Since the center can be in various vibrational states both at the ground level and at the excited level, and since $\Delta r \neq 0$, the transitions occur in a broad band of energies (schematically indicated by vertical dashed lines). Nonradiative return from the excited state to the ground state is possible via the point of intersection, S , of the two curves. This requires an activation energy ΔE , which can be supplied at higher temperatures (thermal quenching of the emission). In the region where the two parabolae intersect, the curve is marked by dashes since the situation is actually more complicated than is indicated here. This is due to interaction between the ground and the excited state at the situation of the intersection point. The present treatment is not invalidated by this.

TABLE 10. Quantum efficiencies (QE) of thallium in 4 matrices

Matrix	Max. absorption nm	Max. excitation nm	Max. emission nm	Oscillator strength, f [35]	QE	Stokes' shift (cm^{-1})
Borax.....	230	248	325	0.072	0.19	12709
Phosphate	212.5	230	300	.080	.23	13726
KCl.....	247	247	300	.074	.5	7153
KBr.....	261	261	320	.097	.44	7064

tures, higher vibrational levels may be occupied. In figure 9, the horizontal lines represent vibrational states. Due to the absorption of radiation of the appropriate wavelength (in this case UV radiation) the center is raised to an excited state. Since the equilibrium distance r_e of the excited state will not in general be equal to that of the ground state, and since the center may be at different vibrational levels, this transition will correspond to a fairly broad absorption band. The fact that the optical absorption corresponds to a vertical transition in figure 9 is attributable to the rapid nature of electronic transitions as compared to vibrational transitions which involve the heavier nuclei (Franck-Condon effect).

Once in an excited state, the system will relax towards the equilibrium state (of the excited level) by dissipation of heat. From this state or nearby levels the system returns to the ground state by emitting radiation. The emission, therefore, also consists of a broad band. Line emission is found only in the exceptional case where the configurational-coordinate curves are identical in shape and have the same equilibrium distance, as in the case of the rare-earth ions. Because of the heat dissipation, the emission always lies at a lower energy than the absorption. This displacement of emission with respect to absorption is known as the Stokes' shift.

With the aid of the simple model in figure 9 (the Mott-Seitz model) one can explain:

- (a) the broad-band character of the emission and absorption of many centers;
- (b) the shift of the emission to lower wavelengths; and,
- (c) the temperature dependence of the emission.

If the equilibrium configuration of the excited state lies outside the curve of the ground state (fig. 10), then, after excitation, the intersection point of both curves is reached before the above-mentioned equilibrium configuration is reached, and the system relaxes nonradiatively to the ground state. No emission is then possible. The radiationless return to the ground state is temperature-independent. This is the model which Seitz proposed to explain the absence of luminescence in certain cases [57]. In other words, the condition for the absence of luminescence is a large difference between the equilibrium distance of the excited state and that of the ground state.

Dexter, Klick, and Russell later proposed a different model [58] which shows that even under less rigorous circumstances than in figure 10, nonradiative transitions to the ground state may occur (fig. 11). The characteristic feature of the situation in figure 11 is that the intersection point S of the two curves is lower than the level reached after excitation. When, after excitation, the system now relaxes while vibrating, to the equilibrium position of the excited state, the intersection point of the two curves is passed. Here too, a temperature-independent, radiationless return to the ground state can take place.

We learn from these models that the difference, Δr , between the equilibrium configuration of the excited

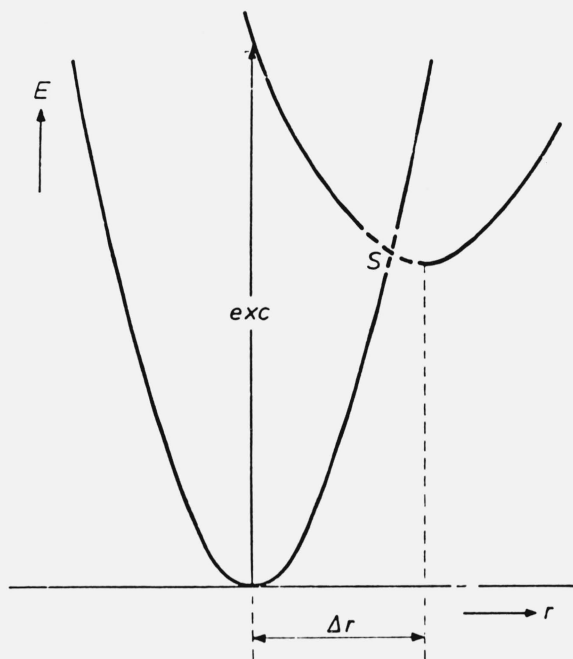


FIGURE 10. The Seitz model for explaining the absence of luminescence; see figure 9. The minimum of the curve for the excited state lies outside the curve for the ground state; luminescence is then not possible.

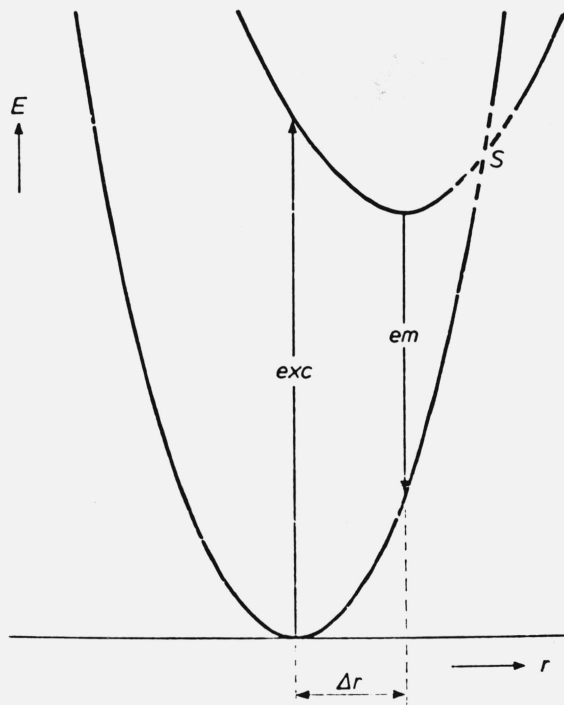


FIGURE 11. The Dexter-Klick-Russel model for explaining a low luminescence efficiency or the absence of luminescence. The intersection point S of the two curves lies below the vibrational level reached after excitation. The nonradiative return to the ground state requires no activation energy (as it did in fig. 9).

state and that of the ground state must be small if luminescence is to occur.

Because of the well-defined and broad fluorescence of thallium in the UV region, we have determined the optimum conditions for preparation of thallium doped alkali halide pellets in phosphate and borate glasses. Also, the dependence of fluorescence efficiency on concentration of Tl^+ was measured. It is shown that the thallium doped pellets and glasses can be used as fluorescence standards. The detailed results of the measurements are given.

A. Thallium Doped Potassium Chloride Disks

Polycrystalline pellets were used [52] as mentioned in the introduction. Such pellets are used in biomedical research for fluorescence measurements.

The optical absorption and fluorescence of alkali halides containing thallium has been widely studied; references can be found in a review paper by Teegarden [51].

The absorption band *A* with maximum around 247 nm in potassium chloride, arises from the spin-forbidden transition $^1A_g \rightarrow ^3T_{1u}$ (corresponding to $^1S_0 \rightarrow ^3P_1$ in a free thallos ion), and is accompanied by the fluorescence with band maximum at 300 nm. Because of large half-widths, the absorption and fluorescence are suitable for quantum-yield studies.

1. Preparation of Disks

Baker Analyzed KCl was ground for 1 h with an automatic mortar and pestle and dried for 48 h at 120 °C. $TlCl$ (BDH Analytical Grade) was then added and the mixture was homogenized in an electric vibrator. In order to obtain low concentrations, the stock mixture was diluted twice with dry KCl powder. Prior to diffusion, the homogenized mixture was ground in an agate mortar with a small amount of triple-distilled water, and redried at 120 °C for 24 h.

As known from previous work [59, 60], only thallium that has undergone diffusion has an absorption band at 247 nm. The completeness of diffusion was checked by heating the mixtures at different temperatures for various periods and measuring the absorbance. The diffusion was then carried out by heating the mixtures at 400 °C for 4 h. Under these conditions, all of the thallium introduced diffuses into the KCl powder.

The absorption measurements were made on a Cary 14 spectrophotometer, with a KCl disk as blank. The effect of the emission on the absorbance readings was negligible, mainly because the solid angle subtended by the photomultiplier was small (0.005 rad), as compared to the full sphere (4π rad) over which emission occurs.

2. Preparation of Quinine Sulfate

Fisher Reagent Grade quinine sulfate was recrystallized from water five times and dried in a vacuum oven at 60 °C. Stock solutions were prepared by dissolving the purified quinine sulfate in 0.1 *N* H_2SO_4 ,

analytical grade. The water used for the stock solutions was distilled, passed through an ion-exchange column, and then doubly distilled from a quartz still. Special low-fluorescence 1 mm quartz cells were used to hold the standard solutions.

3. Emission Measurements

The corrected emission was measured on a Turner 210 spectrofluorimeter in which the regular 1 cm cell was replaced by a special sample holder adapted to hold disks and cells of 1 mm thickness. The sample holder could be rotated to permit continuous variation of the angle of incidence of the exciting light. Because of the optical arrangement of the spectrofluorimeter, it was necessary to place a black-velvet screen between the sample and the collecting mirror to reduce reflections. All measurements were made at constant excitation energy and at room temperature.

Some representative A-band absorption curves are shown in figure 12. A plot of thallium concentration versus absorbance is linear, as can be seen in figure 13.

The oscillator strength, *f*, was calculated from the generalized formula of Smakula, (13), given by Patek (ref. [35], p. 72).

$$f = 0.82 \times 10^{17} \frac{n}{(n^2 + 2)^2} \frac{V}{N} \alpha(E) dE \quad (13)$$

where *n* is the refractive index, $\left(\frac{V}{N}\right)^{-1}$ the concentration of the ions per cm^3 , α the absorbance in cm^{-1} and *E* the energy in electron volts. The refractive index of a KCl crystal was taken from Landolt-Bornstein [61] as 1.59. Multiplying 1.59 by the ratio of the pressed disk density (1.690 g/cm^3) to the crystal density (1.984 g/cm^3) yields an index of refraction value for the pressed disk of 1.57.

The oscillator strength was 0.074 ± 0.002 . Figure 14 shows the corrected emission spectra. The linear concentration dependence of the emission-peak height is shown in figure 15.

The quantum yield was determined by use of eq (11) using quinine sulfate as a standard [52].

The quantum yield of 0.508 for quinine sulfate in 0.1 *N* H_2SO_4 used as a standard was taken from the data of Melhuish at $\lambda_{exc} = 366$ nm. Fletcher showed that the quantum yield was constant to within 5 percent over the wavelength range 240–290 nm, excluding a minimum at 270 nm. The refractive index *n_s* was taken as a weighted mean of the refractive indices of the standard solution and the quartz windows of the cell.

The excitation wavelength for the unknown and the standard was 247.5 nm. The emission-peak height was critically dependent on the angle of incidence of the exciting light, so that the small but inevitable difference of the angles of the sample and reference could cause a considerable error. On the other hand, the shape factor of the emission (ratio of emission-peak area to peak height) was independent of the angle. To eliminate the error, we found the maximum peak height by

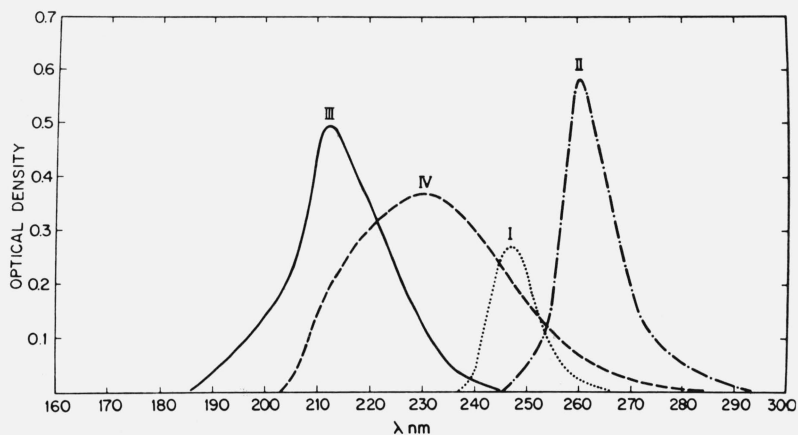


FIGURE 12. A band absorption spectra. I. KCl:Tl⁺, 20 ppm; II. KBr:Tl⁺, 20 ppm; III. Phosphate:Tl⁺, 50 ppm; IV. Borax:Tl⁺, 100 ppm.

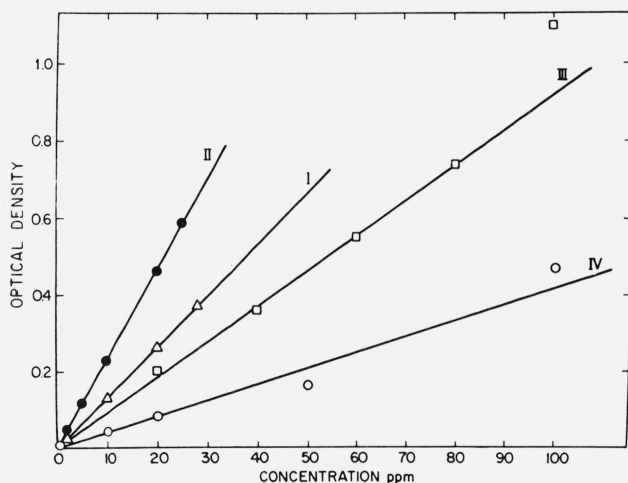


FIGURE 13. Absorbance versus concentration of Tl⁺ in I. KCl; II. KBr; III. Phosphate; IV. Borax.

varying the angle of incidence and multiplied it by the shape factor to obtain the emission-peak area, A.

The quantum yield obtained in this way was 0.50 ± 0.03 .

Pressed polycrystalline KCl:Tl disks differ only slightly in their density from KCl:Tl crystals, and they have the same optical characteristics. All of the thallium diffuses into the polycrystalline disks, and they can therefore be prepared to the predetermined uniform concentration. The linear concentration dependence of the absorbance (fig. 13) gives a check on the reproducibility of the samples, and the agreement of the oscillator strength of the disks with that of the crystals permits their use as a substitute for crystals. From the linear concentration dependence of the emission, it is concluded that the quantum yield is constant over the concentration range 2–30 ppm. Pressed polycrystalline KCl disks doped by diffusion with TlCl can therefore be used as UV luminescence standards at room temperature. The recommended

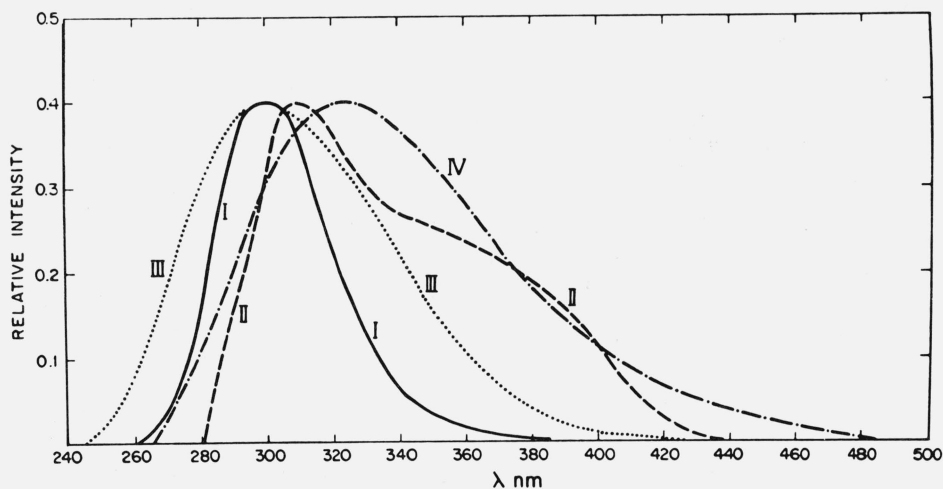


FIGURE 14. Corrected emission spectra I. KCl:Tl⁺; II. KBr:Tl⁺; III. Phosphate:Tl⁺; IV. Borax:Tl⁺.

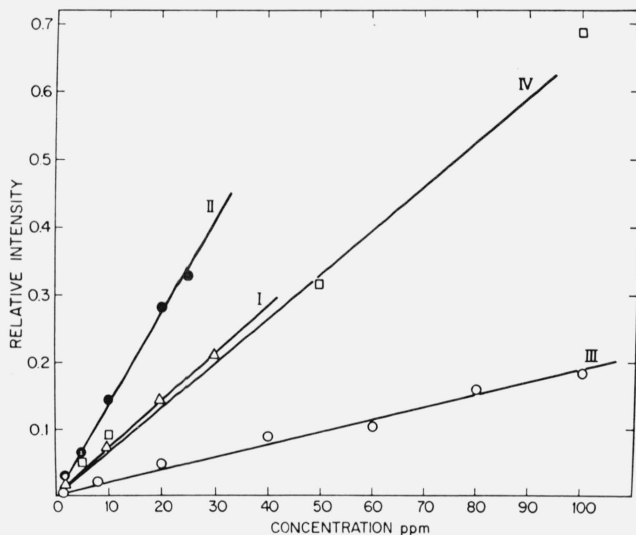


FIGURE 15. The dependence of fluorescence output on Tl^+ concentration: I. KCl; II. KBr; III. Phosphate; IV. Borax.

concentration is 2 ppm, corresponding to 0.624×10^{-6} mol/mol.

B. Thallium-Doped Potassium Bromide Disks

The absorption spectrum of KBr:Tl in polycrystalline disks and single crystals is well known [60, 62] and is presented in figure 12. The concentration dependence of the absorption maximum is presented in figure 13. The corrected emission spectrum of the A band is presented in figure 14. The dependence of fluorescence intensity on concentration is presented in figure 15.

The oscillator strength was calculated by use of Smakula's equation (13), and was found to be 0.097 ± 0.003 . The quantum yield of the A band in KBr:Tl was calculated using KCl:Tl as a standard.

The emission and excitation spectra of the disks were measured on a spectrofluorimeter built in this laboratory, the description of which may be found in reference [36]. The emission spectra were corrected using standard compounds and their reported spectra. To correct for the difference of excitation energy in the standard and the unknown, a correction factor was introduced into eq (11).

The refined formula for the use with this spectrofluorimeter is of the form:

$$\eta_u = \eta_s \frac{F_u A_s d_s \lambda_s n_u^2}{F_s A_u d_u \lambda_u n_s^2} \times \frac{F_s^B F_u^T}{F_s^T F_u^B} \quad (14)$$

in which the parameters have the same meaning as in (11). F_s^B is the relative fluorescence output at peak maximum in the excitation spectrum of the standard measured with our apparatus; F_s^T is the relative fluorescence output at peak maximum in the excitation spectrum of the standard measured on the Turner Model 210 spectrofluorimeter; F_u^B is the output at

peak maximum of the unknown in the excitation spectrum of the standard measured in our apparatus; F_u^T is the output at peak maximum of the unknown measured in the excitation spectrum of the standard on the Turner Model 210 spectrofluorimeter. The density of the pressed KBr disk is 2.67 g/cm^3 .

We used as a standard a KCl:Tl disk with a quantum yield of 0.50. The quantum yield obtained for the KBr:Tl disk is 0.44 ± 0.03 . All data concerning KBr:Tl disks are presented in table 10.

Because of the linear dependence of absorption and emission on the Tl^+ concentration, it is concluded that the quantum yield is independent of the concentration in the 0.5–25 ppm range. Pressed polycrystalline KBr:Tl and KCl:Tl disks can easily be prepared to predetermined concentrations for use as UV fluorescence standards at room temperature. The recommended Tl concentration is 2 ppm, corresponding to 0.837×10^{-6} mol/mol KBr:Tl and 0.624×10^{-6} mol/mol in KCl.

III. Thallium-Doped Glasses

To compare our results in glasses with the corresponding data of alkali halides, we have prepared and measured glasses doped with thallium.

Glasses were prepared from sodium phosphate monobasic and from borax. Glasses, 1 mm thick and 12 mm in diameter were obtained by molding the melt on a tile.

The absorption spectra were recorded on a Cary 14 spectrophotometer using undoped glasses or disks as blanks, and are presented in figure 12. The concentration dependence of the absorption is presented in figure 13.

1. Excitation and Emission Spectra

Excitation and emission spectra were taken on a spectrofluorimeter built in this laboratory [36]. The spectra were corrected with respect to light characteristics and spectral distribution of the photomultiplier by comparison with a similar spectrum taken on the Turner Model 210 spectrofluorimeter using standard compounds (quinine sulfate, fluoresceine, etc.).

The corrected emission spectra are presented in figure 14. The concentration dependence of the emission is presented in figure 15. The quantum efficiencies were obtained by comparison of the glasses with alkali halide-thallium-doped disks using eq (14), the results of which are presented in table 10.

When a pellet or a glass containing thallium is excited through absorption into the A band at room temperature, the emission is composed of two time components, one with a short lifetime of about 25 ns and one with a long component of 400 ns. We have proposed an explanation for the two decay constants [55].

The proposed explanation is as follows: The absorption is from 1S_0 ground state to 3P_1 excited state. The emission occurs also between these two levels and is followed by a Stokes' Shift (see table 10). It is an allowed emission with a short lifetime. However, part

of the population of the 3P_1 level is rapidly depleted by a radiationless process to the metastable 3P_0 state (see fig. 16). This assumption is proven by an experi-

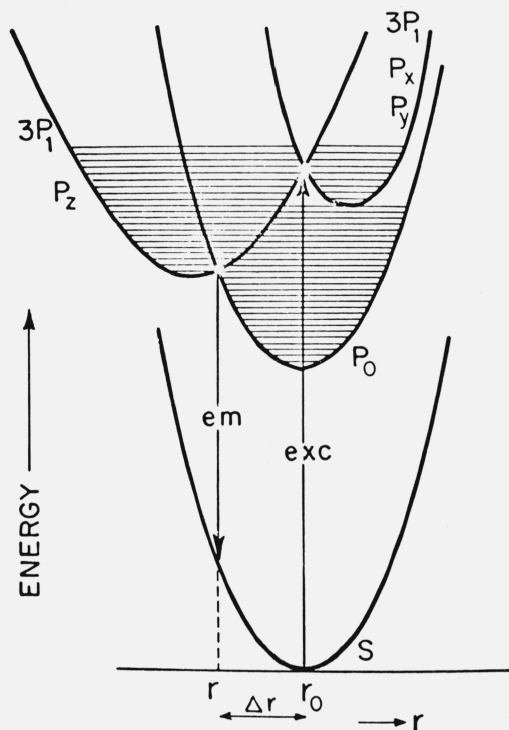


FIGURE 16. Configurational coordinate diagram of Tl^+ in a tetragonal symmetry.

ment of Tomura [63], who had observed a decay of 2–1 ms at 20 K due to this transition. At an elevated temperature, the vibronic modes promote tunnelling from 3P_0 back to 3P_1 . This process occurs with an activation energy of 0.06 eV in KCl. The next process

is the delayed emission from 3P_1 . The rate of this process is the rate of tunnelling which controls the population of 3P_1 . Since both the instant and delayed emission occurs from the 3P_1 state, the wavelength of emission for both decays is the same. Also, the memory of polarization is lost during tunnelling. To determine the quantum yield from the lifetime measurement, additional calculations have to be made because of this delayed fluorescence.

In this mechanism, for all four cases described here, the broadening of the emission in KBr:Tl is due to emission from P_x , P_y and another emission from P_z , and not from P_0 . Splitting of the various P orbitals by the Jahn-Teller effect is stronger the heavier the anion of the host lattice.

The shift of the absorption band to longer wavelength in the order Tl^+ -phosphate, Tl^+ -borax, Tl^+ -KCl and Tl^+ -KBr (also Tl^+ -Kl) indicates that the ligand field acting on Tl^+ increases in the same order. The stronger the ligand field the smaller the difference between the excited and ground state and hence the absorption occurs at longer wavelengths. This also indicates that, in the case of borax, the electrons of the oxygen participating in the thallium-oxygen bond are shifted more to the Tl (stronger polarization of the bond), which is due to stronger electron affinity of phosphorus (0.78 eV) than of boron (0.33 eV).

IV. Glasses Doped by Pb^{2+} , Ce^{3+} , and Cu^+

In a search for standards to cover the fluorescence range from the UV region to the red region, it was found that in addition to thallium doped glasses [64], glasses containing Ce^{3+} [65], Pb^{2+} [66], and Cu^+ [67] lead $^{2+}$ and copper $^+$ are suitable for standards, considering the positions of their emission wavelengths and half bandwidths.

The corrected emission spectra of various glasses containing these ions are presented in figure 17. The

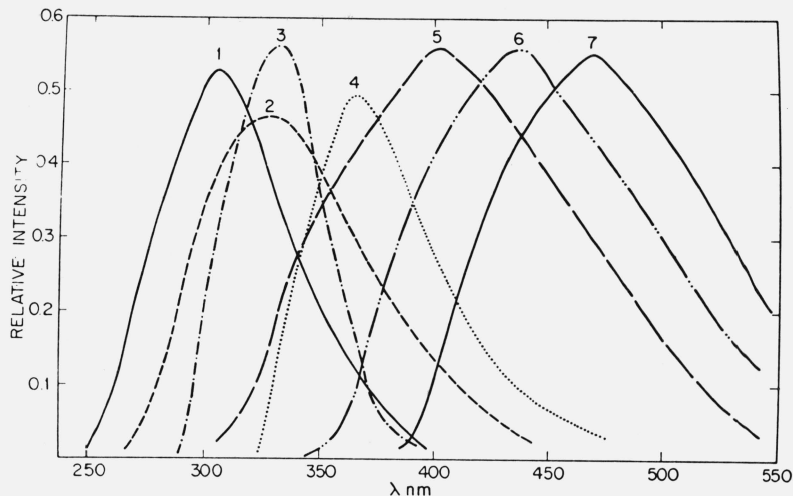


FIGURE 17. Matrix effects on position of emission band of Tl^+ , Ce^{3+} , Pb^{2+} , and Cu^+ . I. Phosphate: Tl^+ ; II. Borax: Tl^+ ; III. Phosphate: Ce^{3+} ; IV. Borax: Ce^{3+} ; V. Borax: Pb^{2+} ; VI. Germanate: Pb^{2+} ; VII Phosphate: Cu^+ .

absorption spectra of Ce^{3+} and Cu^{+} in phosphate glass and Pb^{2+} in borax glass are presented in figure 18. The absorption is linear with concentration in the range measured (1–1000 ppm). The dependence of fluorescence on concentration is linear as shown in figure 19, and this range of concentration can be used for preparation of the standards. The maximum

emission and excitation wave lengths of the glasses and the half bandwidths of the emission are presented in table 11.

The determinations of quantum yields of these glasses are now undergoing research. For these determinations, doped potassium chloride disks are used as standard references [64–67]. For the quantum

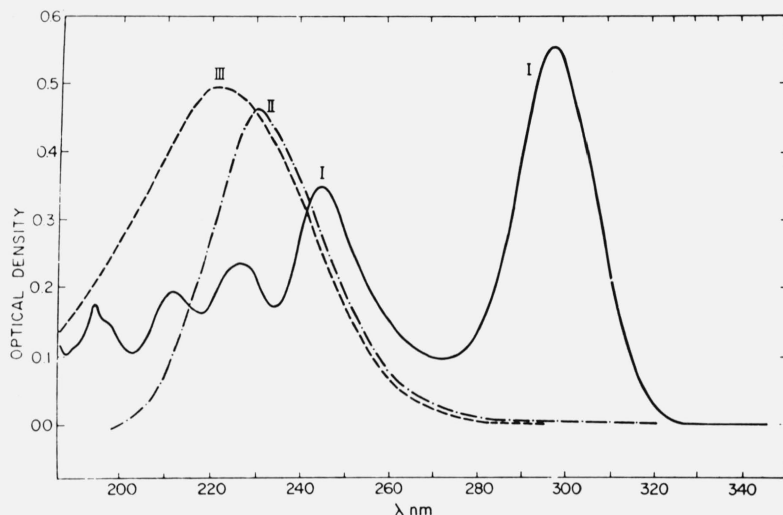


FIGURE 18. Absorption spectrum of I. Ce^{3+} in phosphate, 400 ppm; II. Pb^{2+} in borax, 100 ppm; III. Cu^{+} in phosphate, 50 ppm.

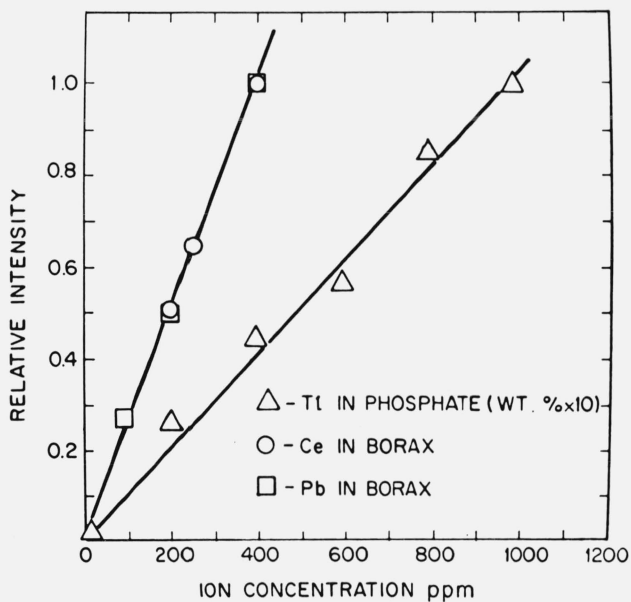


FIGURE 19. The dependence of fluorescence intensity on concentration I. Tl^{+} in phosphate; II. Ce^{3+} in borax; III. Pb^{2+} in borax.

yield determination of Tl in phosphate and borate glasses, and Ce^{3+} in phosphate glasses, quinine sulfate was used as a relative standard [68].

Conclusions

Rare-earth-doped glasses are suggested as relative standards for use with compounds having narrow band excitation and emission of fluorescence. Thallium-doped alkali halides are standards suitable for determination of substances in alkali halide pellets, while thallium doped glasses can be used as standards for glassy substances or liquids in quartz cells. Other varieties of glass standards and pellets are now under investigation. Energy transfer studies which are of great importance in understanding quantum efficiencies will be summarized in a separate review.

The assistance of E. Greenberg in preparation of this paper is gratefully acknowledged. I wish also to express my thanks to Y. Eckstein and L. Boehm for fruitful discussions, and E. Hoffman for providing relevant literature on fluorescence in biomedical systems. I especially wish to express my gratitude to Menis who suggested the topic for this paper.

TABLE 11. Emission and excitation wavelength dependence on matrix for lead, cerium, thallium and copper

Ion	Matrix	Wavelength, nm		Emission half-bandwidths, nm
		Excitation	Emission	
Tl ⁺	KCl	247.5	300	40
Tl ⁺	Phosphate	219.0	302	70
Tl ⁺	Borate	233.0	325	90
Ce ³⁺	Phosphate	297.0	334	55
Ce ³⁺	Borate ^a	310.0	364	80
Ce ³⁺	Borax ^b	311.0	365	65
Ce ³⁺	Silicate	317.0	380	85
Pb ²⁺	Phosphate	241.5	309	70
Pb ²⁺	Borate ^a	261.0	424	140
Pb ²⁺	Borax ^b	241.0	425	165
Pb ²⁺	Germanate	295.0	440	125
Cu ⁺	Phosphate	270.0	445	120

^aMixture of boric acid and boric oxide. ^bSodium borate only.

VI. References

- [1] Parker, C. A., *Photoluminescence of Solutions* (Elsevier Publishing Co., New York, N.Y. 1968); Hercules, D. M. Ed., *Fluorescence and Phosphorescence Analyses*. (Interscience Publishing Co., New York, N.Y., 1966); B. Becker, R. S., *Theory and Interpretation of Fluorescence and Phosphorescence* (John Wiley & Sons, Inc., New York, N.Y., 1969).
- [2] White, C. E., and Argaver, R. J., *Fluorescence Analysis* (M. Dekker, Inc., New York, N.Y. 1970); Berlman, I. B., *Handbook of Fluorescence Spectra of Aromatic Molecules*, (Academic Press, New York, N.Y., 2nd Edition 1971).
- [3] Demas, J. N., and Crosby, G. A., *J. Phys. Chem.* **75**, 991 (1971).
- [4] Edelman, G. M., and McClure, W. O., *Accounts. Chem. Res.* **1**(3), 65 (1968).
- [5] Strayer, L., *Science* **162**, 526 (1968).
- [6] Rinder-Knecht, H., *Nature* **193**, 167 (1962).
- [7] Hartley, B. S., and Massey, V., *Biochim. Biophys. Acta* **21**, 58 (1956).
- [8] Deyl, Z., and Rosmus, J., *J. Chromatogr.* **20**, 514 (1965).
- [9] Pataki, G., and Strasky, E., *Chimia* **20**, 361 (1966).
- [10] Chen, R. F., *Arch. Biochem. Biophys.* **120**, 609 (1967).
- [11] Moye, H. A., and Winefordner, J. D., *J. Agr. Food Chem.* **13**, 516 (1965).
- [12] Staniland, L. N., *J. Agr. Eng. Res.* **4**, 110 (1959).
- [13] Staniland, L. N., *J. Agr. Eng. Res.* **5**, 42 (1960).
- [14] Udenfriend, S., *Fluorescence Assay in Biology and Medicine* (Academic Press, New York, N.Y., Vols. I and II, 1962, 1969).
- [15] Van Duuren, B. L., *J. Natl. Cancer Inst. Monograph No.* 9, 135 (1962).
- [16] Van Duuren, B. L., *Acta Unio Intern. Contra Cancrum* **19**, 524 (1963).
- [17] Konev, S. V., *Fluorescence and Phosphorescence of Proteins and Nucleic Acids*, (Plenum Press, New York, 1967), p. 171.
- [18] Booth, J., et al., *J. Chem. Soc.* 598 (1954).
- [19] De Santis, F., et al., *Nature* **191**, 900 (1961).
- [20] Liquori, A. M., et al., *J. Mol. Biol.* **5**, 521 (1962).
- [21] Cook, J. M., *J. Chem. Soc. London*, 1210 (1950).
- [22] Sawicki, E., et al., *Talanta* **14**, 431 (1967).
- [23] Van Bertalanffy, L., et al., *Cancer* **11**, 873 (1958).
- [24] Rubin, M., *Fluorimetry in Clinical Chemistry*, American Instrument Co., Silver Spring, Maryland.
- [25] Phillips, R. E., Ed., *Manual of Fluorimetric Clinical Procedures*, G. K. Turner Assoc., Inc., Palo Alto, California.
- [26] Van Duuren, B. L., and Bardi, C. E., *Anal. Chem.* **35**, 2198 (1963).
- [27] Winefordner, J. D., and St. John, P. A., *Anal. Chem.* **35**, 2211 (1963).
- [28] Samson, J. A. R., *Techniques of Vacuum Ultraviolet Spectroscopy* (John Wiley & Sons, Inc., New York, 1967), p. 212-216.
- [29] Brill, A., *Luminescence of Organic and Inorganic Materials* (John Wiley & Sons, Inc., New York, N.Y. 1962), p. 477.
- [30] Birks, J. B., and Dyson, D. J., *Proc. Roy. Soc.* **275A**, 135 (1963).
- [31] Seybold, P. G., Gouterman, M., and Callis, J., *Photochemistry and Photobiology* **9**, 229 (1969).
- [32] Lewis, G. N., and Kasha, M., *J. Am. Chem. Soc.* **67**, 994 (1945).
- [33] Strickler, S. J., and Berg, R. A., *J. Chem. Phys.* **37**, 814 (1962).
- [34] Wybourne, B. G., Ed., *Spectroscopic Properties of the Rare Earths* (Interscience Publ., New York, N.Y. 1965).
- [35] Patek, K., *Glass Lasers*, Edwards, J. G., Ed., London (Butterworth & Co., 1970).
- [36] Reisfeld, R., Honigbaum, A., Michaeli, G., Harel, L., and Ish-Shalom, M., *Israel J. Chem.* **7**, 613 (1970).
- [37] Reisfeld, R., Greenberg, E., Kirshenbaum, L., and Michaeli, G., *Proc. 8th Rare Earth Conference* **2**, 743 (1970).
- [38] Reisfeld, R., and Hornadaly, J., *Proc. 9th Rare Earth Conference*, **1**, 123 (1971).
- [39] Reisfeld, R. and Eckstein, Y., *Solid State Chem.* **5**, 174 (1972).
- [40] Reisfeld, R., Velapoldi, R. A., Boehm, L., and Ish-Shalom, M., *J. Phys. Chem.* **75**, 3981 (1971).
- [41] Reisfeld, R., Velapoldi, R. A., and Boehm, L., *J. Phys. Chem.* **76**, 1293 (1972).
- [42] Velapoldi, R. A., Reisfeld, R., and Boehm, L., *Proc. 9th Rare Earth Res. Conf.* **2**, 488 (1971).
- [43] Reisfeld, R., and Greenberg, E., *Anal. Chem.* **47**, 155 (1969).
- [44] Turner, G. K., *Science* **146**, 183 (1964).
- [45] Fletcher, A. N., *J. Mol. Spectry.* **23**, 221 (1967).
- [46] Reisfeld, R., Greenberg, E., Velapoldi, R. A., and Barnett, B., *J. Chem. Phys.* **56**, (4) 1698 (1972).
- [47] Reisfeld, R., Glasner, A., and Mustaki, A., *Proc. Int. Colloqu. Optic and Spectroscopic Phenomena in Ionic Crystals*, Bucharest, 1968; Mustachi, A., Reisfeld, R., and Glasner, A., *Israel J. Chem.* **7**, 627 (1970).
- [48] Reisfeld, R., and Biron, E., *Talanta* **17**, 105 (1970).
- [49] Reisfeld, R., Arye, Z. Gur., and Greenberg, E., *Anal. Chim. Acta* **50**, 249 (1970).
- [50] Reisfeld, R., and Eckstein, Y., *Anal. Chim. Acta* **56**, 461 (1971).
- [51] Teegarden, T., in *Luminescence of Inorganic Solids*, Goldberg, P., Ed. (Academic Press, New York, N.Y., 1966), p. 83.
- [52] Reisfeld, R., Honigbaum, A., and Velapoldi, R. A., *J. Opt. Soc. Am.* **61**, 1422 (1971).
- [53] Scott, A. B., and Hu, K. H., *J. Chem. Phys.* **23**, 1830 (1955).
- [54] Sturge, M. D., *Solid State Physics* **20**, 91 (1967).
- [55] Reisfeld, R., Greenberg, E., Deinum, T., Werkhoven, C. J., and van Voorst, J. D. W., to be published.
- [56] Blasse G., and Brill, A., *Philips Technical Review* **31**, 304 (1970).
- [57] Seitz, F., *Trans. Faraday Soc.* **35**, 74 (1939).
- [58] Dexter, D. L., Klick, C. C., and Russel, G. A., *Phys. Rev.* **100**, 603 (1955).

- [59] Glasner A., and Reisfeld, R., J. Phys. Chem. Solids **18**, 345 (1961).
- [60] Glasner, A., Rejoan, A., and Reisfeld, R., J. Phys. Chem. Solids **19**, 331 (1961).
- [61] Landolt-Bornstein, Zahlenwerte und Funktionen, Bd. **2**, Teil 8, Optische Konstanten (Springer, Berlin, 1962).
- [62] Reisfeld, R., and Honigbaum, A., 1972, unpublished results.
- [63] Tomura, M., and Nishimura, H., J. Phys. Soc. Japan, **21**, 2081 (1966).
- [64] Reisfeld, R., and Morag, S., J. Appl. Phys. Letters **21**, 57 (1972).
- [65] Reisfeld, R., Hormodaly, J., and Barnett, B., Chem. Phys. Letters.
- [66] Reisfeld, R., and Lieblich, N., unpublished results.
- [67] Reisfeld, R., and Kosloff, R., unpublished results.
- [68] Reisfeld, R., Velapoldi, R. A., and Greenberg, E., unpublished results.

(Paper 76A6-746)